Gravity Compensation and Design Modification of a Scapulohumeral Exoskeleton Joint

A Thesis

Presented in Partial Fulfillment of the Requirements for the

Degree of Master of Science

with a

Major in Mechanical Engineering

in the

College of Graduate Studies

University of Idaho

by

Jacob R. Brower

Approved by:

Major Professor: Joel Perry, Ph.D.

Committee Members: Eric Wolbrecht, Ph.D.; Daniel Robertson, Ph.D.

Department Administrator: Gabriel Potirniche, Ph.D.

May 2023

Abstract

This thesis investigates the design of PRISM (Parallel Rotation mechanism for the Inclusion of Scapulothoracic Motion) for the exoskeleton BLUE SABINO (BiLateral Upper-extremity Exoskeleton for Simultaneous Assessment of Biomechanical and Neuromuscular Output). PRISM (previously known as PANDORA) is the portion of BLUE SABINO that is responsible for providing shoulder protraction/retraction and elevation/depression, known as scapulohumeral rhythm. Shawn Trimble performed the original design work (Trimble, 2016). A key function of PRISM is gravity assistance. The joint responsible for shoulder elevation/depression must lift the entire exoskeleton. A gravity assistance mechanism should reduce torque requirements, maintain actuator placement, consider ergonomics, and improve safety. This process is split into two portions: designing spring attachments and selecting an appropriate spring. Thousands of springs are evaluated to discover the single spring that minimizes the change in force as PRISM actuates, minimizes the spring length, and maximizes the potential force in the spring. A structural goal of most exoskeletons is to minimize both mass and deflection. Components within PRISM that contribute to both mass and deflection (parts 2004, 2009 and 2010) were redesigned and evaluated through FEA within SolidWorks. The best design has a deflection of 0.2415 mm and a mass of 14.086 kg. This a 39% decrease in deflection and a 3% increase in mass with respect to the original design.

Acknowledgments

First, I would like to extend my gratitude to my major professor, Dr. Joel Perry. I appreciate your insight in the design work of guiding me towards graduation and working with me as I transitioned to remote work. Your hard work establishing BLUE SABINO at the University of Idaho has provided an opportunity for myself and so many other students. Your insight was essential in solving errors in both design and simulation. I am also thankful for your editing of this thesis, and your willingness to help me reach deadlines on short notice.

I would also like to acknowledge Dr. Eric Wolbrecht for constantly providing insight that is rooted in controls. The feedback was helpful in improving design and forcing myself to approach the design through a different lens.

To my committee members, Dr. Joel Perry, Dr. Eric Wolbrecht, and Dr. Daniel Robertson, thank you for taking the time to assist in editing this paper, attend my defense, and recommend improvements to both my thesis and research.

Finally, thank you to the BLUE SABINO team for working beside me over the last few years. I have enjoyed working with all of you over my time researching for BLUE SABINO. Thank you as well to the many graduate students that completed their time on this project before I began. All your research has been essential in creating BLUE SABINO as it is today.

Dedication

I dedicate this work to my family.

To my parents Jeff and Judy, thank you for always demonstrating and modeling a strong work ethic. Even though I struggled to appreciate it at the time, I respect you both for the work you have done throughout your careers and wish you the best in your retirement. Thank you for continuing to push me throughout my academics.

To my siblings Brad and Jacque, thank you for being my biggest supporters for as long as I can remember. I know I can always count on you guys, and your endless support has not gone unnoticed.

To my wife Nicole, thank you for being with me throughout this process. I appreciate you listening to me as I navigated problems and continuing to support me as I struggled. But most importantly, thanks for telling me what I needed to hear and reminding me to accept it, graciously.

Table of Contents

List of Tables

List of Figures

Chapter 1: Introduction

This thesis presents research on the development of PRISM (Parallel Rotation mechanism for the Inclusion of Scapulothoracic Motion). PRISM is a portion of an exoskeleton being created for post-stroke rehabilitation and therapy.

1.1 Stroke Background

Stroke occurs when a portion of the brain is deprived of oxygen after a ruptured blood vessel (hemorrhage) or a blockage (ischemia). If oxygen is not restored within minutes, the rupture or blockage results in brain cell death (necrosis) and loss of function. Preliminary symptoms of a stroke include facial droop, muscle weakness, and difficulty in forming or understanding words. Long term, brain damage from stroke can cause losses of memory, speech, and muscle control.

Stroke is one of the leading causes of disability in the United States (Tsao et al., 2022). Based on a National Hospital Care Survey in 2014, 39.8% of people who suffered a stroke were discharged to an inpatient rehabilitation facility, skilled nursing facility, or home with an organized health service (Jackson & Chari, 2019). In 2009, there were nearly a million stroke hospitalizations reported to U.S. hospitals (Hall et al., 2012), and as of 2018, 7.6 million people in the U.S. claim to have suffered a stroke at some point in their life (Tsao et al., 2022). More people are surviving strokes which is leading to a greater number of people living with stroke-related impairments (GBD 2016 Stroke Collaborators, 2019). The average age of the American population is also increasing. It is projected that in 2034 elderly (65 years of age and over) will outnumber children (under 18 years of age) for the first time in U.S history (Vespa, 2018). The increasing number of elderly could directly lead to higher stroke prevalence, especially considering that two-thirds of all strokes happen in people aged 65 and over (Hall et al., 2012). While an improved survival rate and longer life are beneficial, they lead to a greater number of stroke survivors in need of therapy. The decreasing death rate is from a variety of factors, but a noticeable factor is improved blood pressure control leading to lower blood pressures (Lackland et al., 2014). Still, stroke is the 5th leading cause of death in the U.S. (Murphy et al., 2020).

Post-stroke rehabilitation and therapy begins shortly after suffering a stroke. The first 1-3 months are the most important recovery period for a stroke survivor with greatest

recovery occurring in this timeframe (Zeiler, 2019). This illustrates the importance of having accessible therapy available to stroke survivors immediately after suffering a stroke. Therapy involves the rewiring and retraining of the brain to complete tasks with healthy brain cells. Recovery from a stroke is not guaranteed: 40% of stroke survivors experience moderate to severe impairments, 25% recover with minor impairments, 10% recover immediately, and 10% require a nursing home or long-term care facility (American Heart Association, 2019). There is always a need for better therapy practices, especially with a rising need for therapy. One type of therapy that has been established to fill this need is robotic therapy. Robot-assisted training for upper-limb functionality has been established as beneficial in an evaluation of all rehabilitation processes (Langhorne et al., 2011). This therapy is primarily performed through devices known as rehabilitation robots.

1.2 Rehabilitation Robotics

Historically, the primary use of robotics has been to improve safety and/or productivity. Common applications were for tasks deemed too dirty, dangerous, or distant for humans which resulted in little proximity between robots and humans (Krebs & Volpe, 2013). This approach to robotics changed in the late 1980s and early 1990s to include robot-human interaction in the hope of improving human performance, including the eventual investigation into human rehabilitation. The primary goal of robotic rehabilitation was to replace the physician with completely automated therapy which has not occurred. Instead, the attempts provided a new tool to researchers and therapists, as a method to precisely quantify therapy results during exercise (Colombo & Sanguineti, 2018). These early rehabilitation robotic discoveries have led to decades of lower-limb and upper-limb exoskeleton development.

1.2.1 Upper-Limb Exoskeletons

Upper-limb exoskeletons are unique therapeutic devices that can apply assistance and allow for quantifiable data during exercise. Exoskeletons primarily treat the shoulder joint as a 3-Degree-Of-Freedom (3-DOF) stationary spherical (i.e., ball-and-socket) joint. These 3-DOF devices include the motions of shoulder flexion/extension, abduction/adduction, and internal/external rotation while not allowing for shoulder protraction/retraction or elevation/depression. This arrangement simplifies both design and control. In a survey of

over 120 robotic devices for upper-limb rehabilitation, only 4 of 64 shoulder movement devices directly addressed horizontal or vertical displacement of the shoulder (Maciejasz et al., 2014). These included MAG, Pneu-WREX, the ESTEC exoskeleton, and IntelliARM. MAG is a 6-DOF freedom exoskeleton with 4-DOF in the shoulder including elevation/depression but not protraction/retraction (Carignan et al., 2007). Pneu-WREX applies pneumatics to actuate "forward/backward clavicle rotation" which is another description of horizontal shoulder displacement (Wolbrecht et al., 2006). The exoskeleton developed by the European Space Research and Technology Centre (ESTEC) incorporated motion of the shoulder girdle (elevation/depression and protraction/retraction) as well as flexion/extension, abduction/adduction, and internal/external rotation (Schiele & van der Helm, 2006). IntelliARM is an exoskeleton that actively actuates for 4-DOF in the shoulder (flexion/extension, abduction/adduction, internal/external rotation, and elevation/depression) and passively accounts for protraction/retraction through 2 other degrees of freedom in the shoulder (Park et al., 2008). Harmony (Kim & Deshpande, 2017) and MEDARM (Ball et al., 2007) are two additional exoskeletons not included in the review that also actively account for 5-DOF shoulder movement. These six exoskeletons are presented in Figure 1-1.

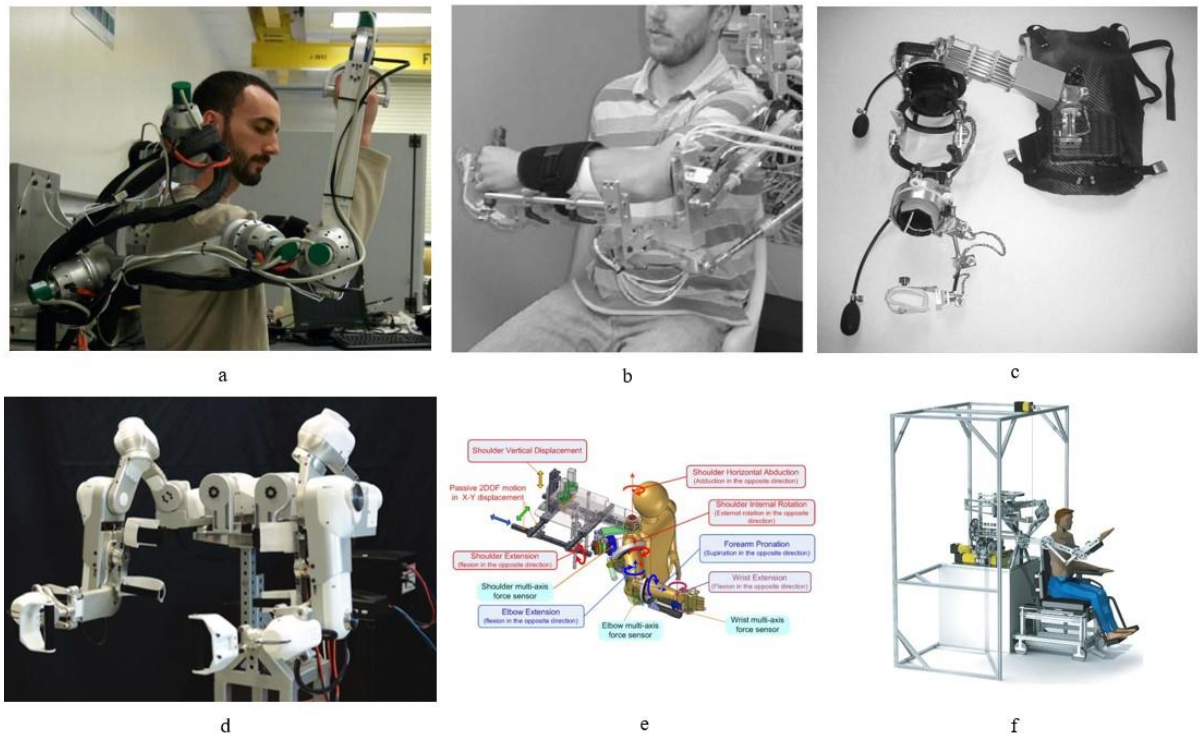

Figure 1-1 Exoskeletons with DOF for shoulder elevation/depression and/or protraction/retraction. These exoskeletons are (a) MGA (Carignan et al., 2007), (b) Pneu-WREX (Wolbrecht et al., 2006), (c) ESTEC exoskeleton (Schiele & van der Helm, 2006), (d) Harmony (Kim & Deshpande, 2017), (e) IntelliARM (Park et al., 2008), and (f) MEDARM (Ball et al., 2007).

Another example of upper-limb exoskeletons is found in the EXO-UL series. These exoskeletons have been under development through the guidance of Jacob Rosen, the Director of the UCLA Bionics Lab. The series began with 1-DOF and 3-DOF proof-of-concept designs of the exoskeleton known as EXO-UL1 and EXO-UL3, respectively. The devices were expanded into a 7-DOF cable-actuated dexterous exoskeleton for neurorehabilitation (CADEN-7, also known as EXO-UL7) which is shown in Figure 1-2. These degrees of freedom include 3-DOF in the shoulder (flexion/extension, abduction/adduction, and internal/external rotation), 1-DOF in the elbow (flexion/extension), 1-DOF in the forearm (pronation/supination), and 2-DOF in the wrist (extension/flexion and radial/ulnar deviation) with shoulder flexion/extension and abduction/adduction combined for singularity placement (Perry et al., 2007). The next iteration of the EXO-UL series, EXO-UL8, added a hand gripper. The cable actuation was also replaced with a combination of harmonic drives, DC motors, and belts (Shen et al., 2018). A continuation and expansion of the EXO-UL series is occurring through an upper-limb exoskeleton named BLUE SABINO.

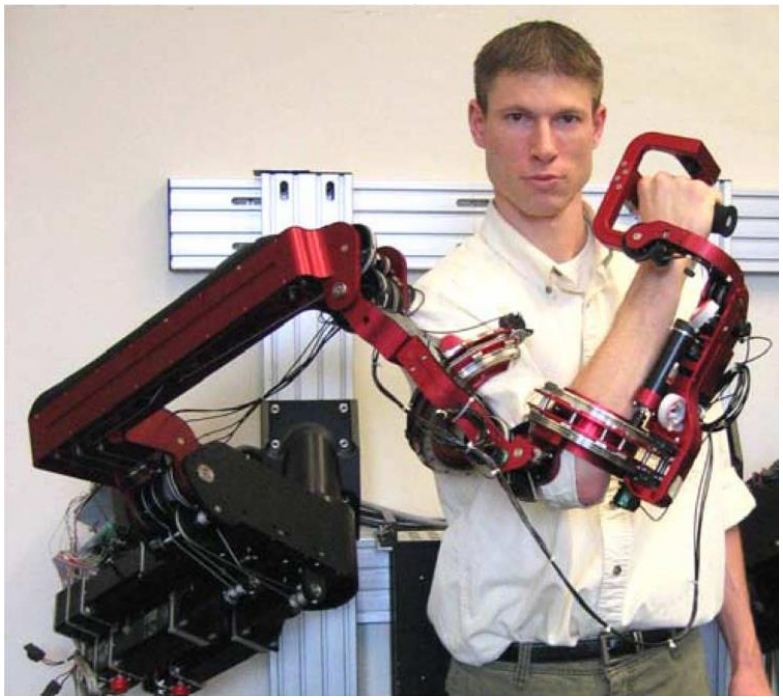

Figure 1-2 The EXO-UL7 (CADEN-7) exoskeleton. The 7-DOF exoskeleton is within the EXO-UL series of exoskeletons. The exoskeleton still incorporates cables for actuation rather than later implemented harmonic drives (Perry et al., 2007).

1.2.2 BLUE SABINO

BLUE SABINO (BiLateral Upper-extremity Exoskeleton for Simultaneous Assessment of Biomechanical and Neuromuscular Output) is an exoskeleton currently under development at the University of Idaho. This system is designed for better therapeutic assessment and rehabilitation for survivors of stroke suffering from upper-limb disability. The device records extensive metrics through electroencephalography (EEG), electromyography (EMG), force-torque sensors, and harmonic drives. This allows for mapping of brain waves to resulting motion in a non-invasive process: EEG provides brain measurements, EMG measures muscle activation, force-torque sensors record force interactions between the human and exoskeleton, and the harmonic drives actuate the movement (Perry et al., 2019).

The development of this 30-DOF dual-arm exoskeleton contains two symmetric 15-DOF arms, one left arm and one right arm. Both 15-DOF sides are composed of a 9-DOF arm exoskeleton developed through the University of Idaho and a 6-DOF hand exoskeleton developed through the University of California Los Angeles. The 9-DOF portion of the arm exoskeleton is composed of a 2-DOF shoulder mechanism, a 3-DOF upper-arm mechanism,

a 2-DOF forearm mechanism, and a 2-DOF wrist mechanism. The initial CAD of BLUE SABINO is shown in Figure 1-3.

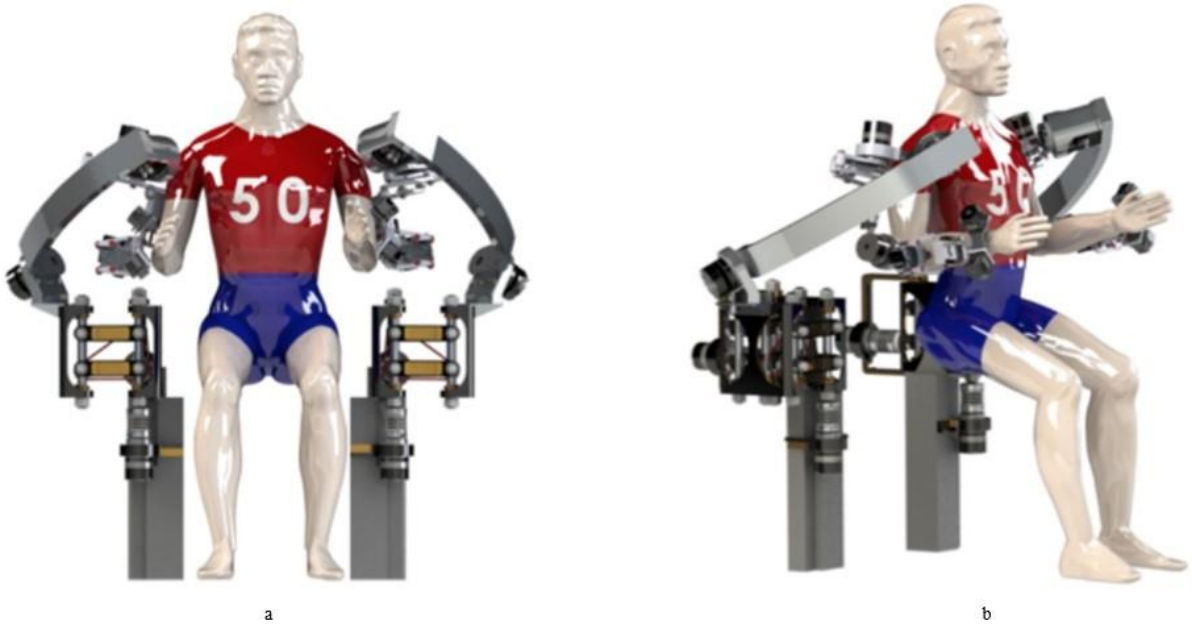

Figure 1-3 Renders of BLUE SABINO. Initial design work of expanding the EXO-UL series into BLUE SABINO. Designs are from 2016 and include (a) a front view and (b) an isometric view (Trimble, 2016).

A goal of BLUE SABINO is the design and development of a device that incorporates two additional DOFs at the shoulder for elevation/depression and protraction/retraction. The addition of horizontal and vertical translation of the shoulder joint allows for greater mobility and reduces forces between the human and exoskeleton.

1.2.3 PRISM

A dual four-bar mechanism called PRISM has been included in the design of BLUE SABINO to enable scapulohumeral rhythm and translation of the shoulder joint. PRISM is an acronym for Parallel Rotation mechanism for the Inclusion of Scapulothoracic Motion. Scapulohumeral rhythm describes the relationship between the scapula and humerus. PRISM (formerly known as PANDORA, Parallel Positioning Dual Four-Bar Mechanism) is composed of two adjacent four-bar mechanisms. Planar four-bar mechanisms are composed of four links: ground, input, output, and floating. The ground link remains stationary and connects to the input and output pivot points. The input link is the driving link that actuates the system through an applied torque. The output link is the driven link that produces the resultant motion. The floating link connects the input and output links while also moving.

These linkages combine to result in a one degree-of-freedom mechanism. The more commonly known “parallelogram” is a specific type of four-bar mechanism in which the input and output links are the same length and angle, and the ground and floating links are the same length. PRISM is designed as a parallelogram in 2-dimensions with two sets of planar parallel four-bar link systems, one set in each the vertical and horizontal direction. The length of the input and output links are set to 152.4 mm to account for human clavicle length, and the range-of-motion is 15-deg for protraction, retraction, elevation, and depression (Hill et al., 2019). Both Joints 1 and 2 have 30-deg of total actuation range. The PRISM design in Figure 1-4 was originally designed by Shawn Trimble (Trimble, 2016).

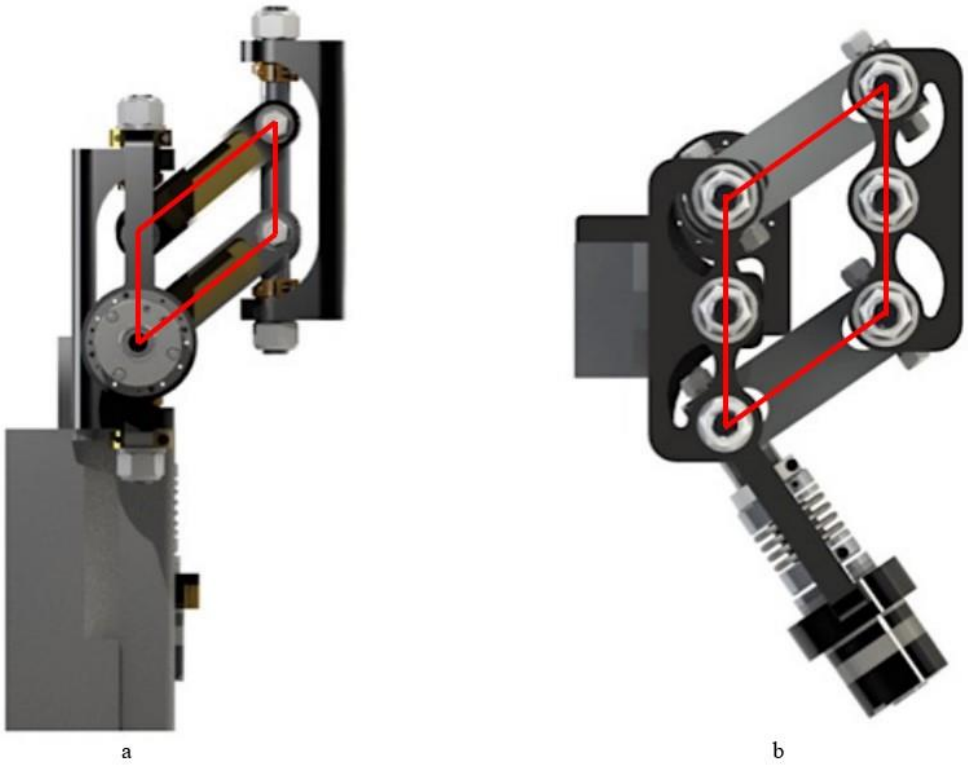

Figure 1-4 Renders of PRISM (previously known as PANDORA). Initial design of the portion of BLUE SABINO responsible for shoulder elevation/depression and shoulder protraction/retraction. Both 4-bar mechanisms are outlined in red. Designs are from 2016 and include (a) a side view illustrating elevation and (b) a top view illustrating protraction (Trimble, 2016).

1.3 Gravity Compensation

Gravity compensation is the process of counteracting gravitational forces that act on an object or mechanism. A simple form of compensating for gravity is achieved through basic counterbalancing. This is the foundation of measurement equipment such as traditional

scales for weighing objects. Counterbalancing is not an effective option for low space, high weight situations, which is often the case with exoskeletons. Another approach to gravity compensation is balancing the load with springs. Springs have the benefit of being able to apply larger forces in small spaces without large amounts of weight and inertia. With the right design and implementation, springs are a simple and effective approach to statically balance loads.

1.3.1 Zero-Free-Length Springs

A common theorized approach to gravity balancing is through a theoretical component known as a zero-free-length spring. Springs require some initial tension before deflection occurs. Zero-free-length springs do not require initial tension before deflection, thus, apply zero force at zero length. A simple zero-free-length spring mechanism in robotics attaches one end of the spring to the link and the other end to a fixed location in line with the link rotation axis as shown in Figure 1-5. This mechanism, when using a zero-free-length spring, results in a sum of moments about the link pivot point with the following relationship:

$$mgr_m = rka \tag{1}$$

where m is the mass, g is acceleration due to gravity, r_m is the distance to the center of mass from the pivot, r is the distance to the spring attachment from the pivot, k is the spring constant, and a is the vertical distance between the pivot and fixed end of the spring.

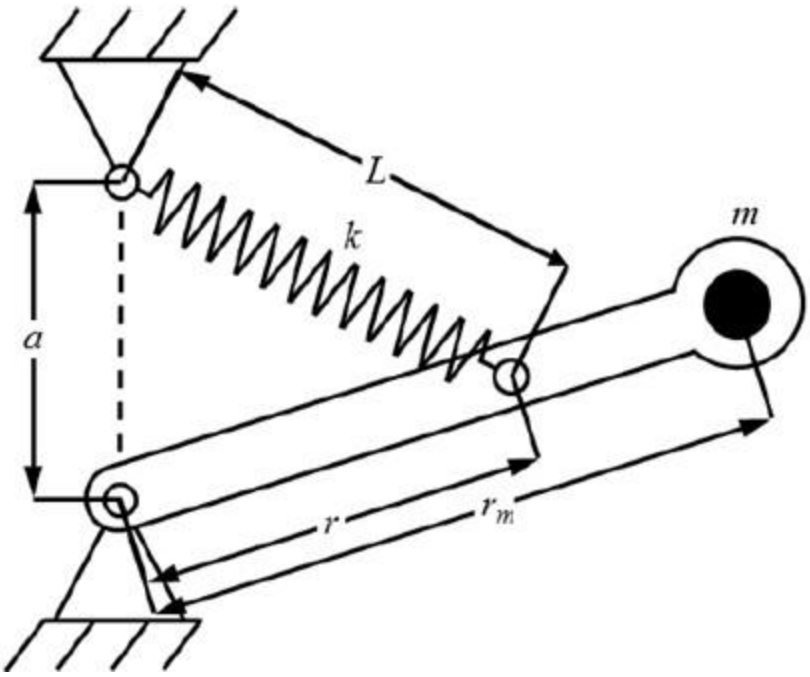

Figure 1-5 Basic gravity equilibrator. The simplest approach to a zero-free-length spring gravity compensation system. The theoretical system utilizes a zero-free-length spring to gravity balance a 1-DOF link (Herder, 2001).

Careful selection of *r*, *k*, and *a* can gravity balance any combination of r_m and *m*, but r_m and *m* must be precisely known which is often not the case. This relationship is dependent on a perfect zero-free-length spring, and perfect zero-free-length springs do not exist. Most readily available springs have a free length that amounts to 70-90% of the initial length (Herder, 2001). Options to achieve static gravity balancing with a spring include increasing the initial tension of the spring or altering the design so the free length is not as affected, for example, through pulleys. Several examples of implementing pulleys are theorized in Figure 1-6. This simple proposed method of gravity balancing applies to a single link system, while BLUE SABINO has significantly more links and requires a more complex approach.

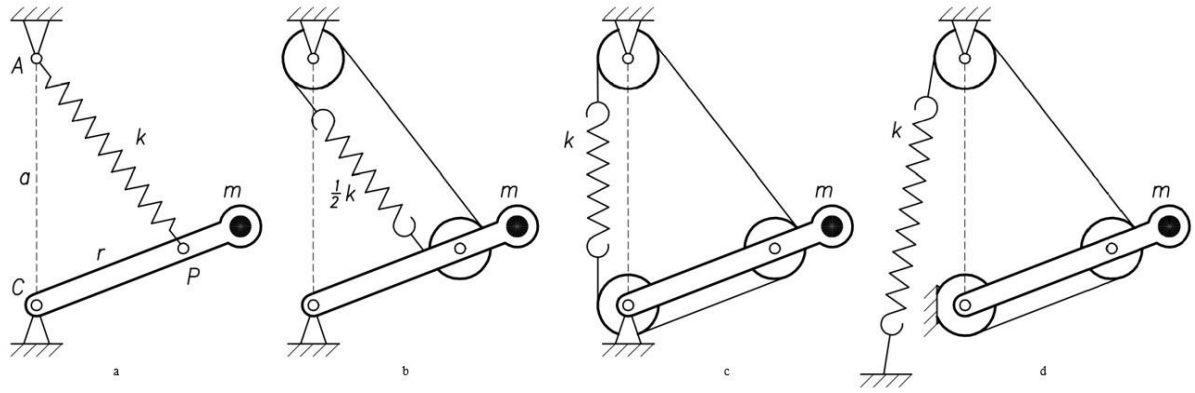

Figure 1-6 Gravity balancing with springs and pulleys. Setups include (a) a basic gravity equilibrator without pulleys, (b) a two-pulley gravity balance system, (c) a three-pulley gravity balance system, and (d) a three-pulley gravity balance system with the spring fixed to the ground. Pulleys are implemented to minimize the change in length of the spring. Previous design concepts were based off configuration (d) (Herder, 2001).

1.3.2 Motivation for Gravity Balancing

Gravity balancing exoskeletons provides benefits in both safety and design. Exoskeletons without passive gravity balancing primarily rely on motors to support the weight of the exoskeleton. Motor failure can result in large forces on the human in the exoskeleton. These forces are highly dependent on the weight of the exoskeleton as well as physical safety stops. Perfect passive gravity balancing would provide constant gravitational assistance and allow for motors to only apply torque to actuate the exoskeleton rather than a combination of gravity assistance and actuation. Imperfect gravity balancing is also beneficial in reducing torque requirements in both static and dynamic loading conditions. Optimal performance for backdrivable motors in exoskeletons supplies an average torque of zero with similar time spent applying torque in each direction (positive and negative torque).

BLUE SABINO has several joints that could benefit from gravity balancing. Links and joints located closer to the base link are more likely to need gravity compensation. These joints are responsible for moving and supporting all distal parts of the exoskeleton. A great example of this is found in BLUE SABINO, specifically PRISM. The first two joints in PRISM are responsible for shoulder protraction/retraction and shoulder elevation/depression. Joint 2, shoulder elevation/depression, lifts and lowers the entire exoskeleton upon movement and supports the entire exoskeleton in a static phase. This would suggest that joint 2 benefits from gravity balancing. An initial gravity balance system has been designed (Trimble, 2016). The decision to gravity balance joint 2 and whether to compensate for

gravity in other joints has already been supported in an analysis of activities-of-daily-living (ADL) movements (C. Bitikofer, 2018; C. K. Bitikofer et al., 2018). The results of this study are illustrated in Figure 1-7.

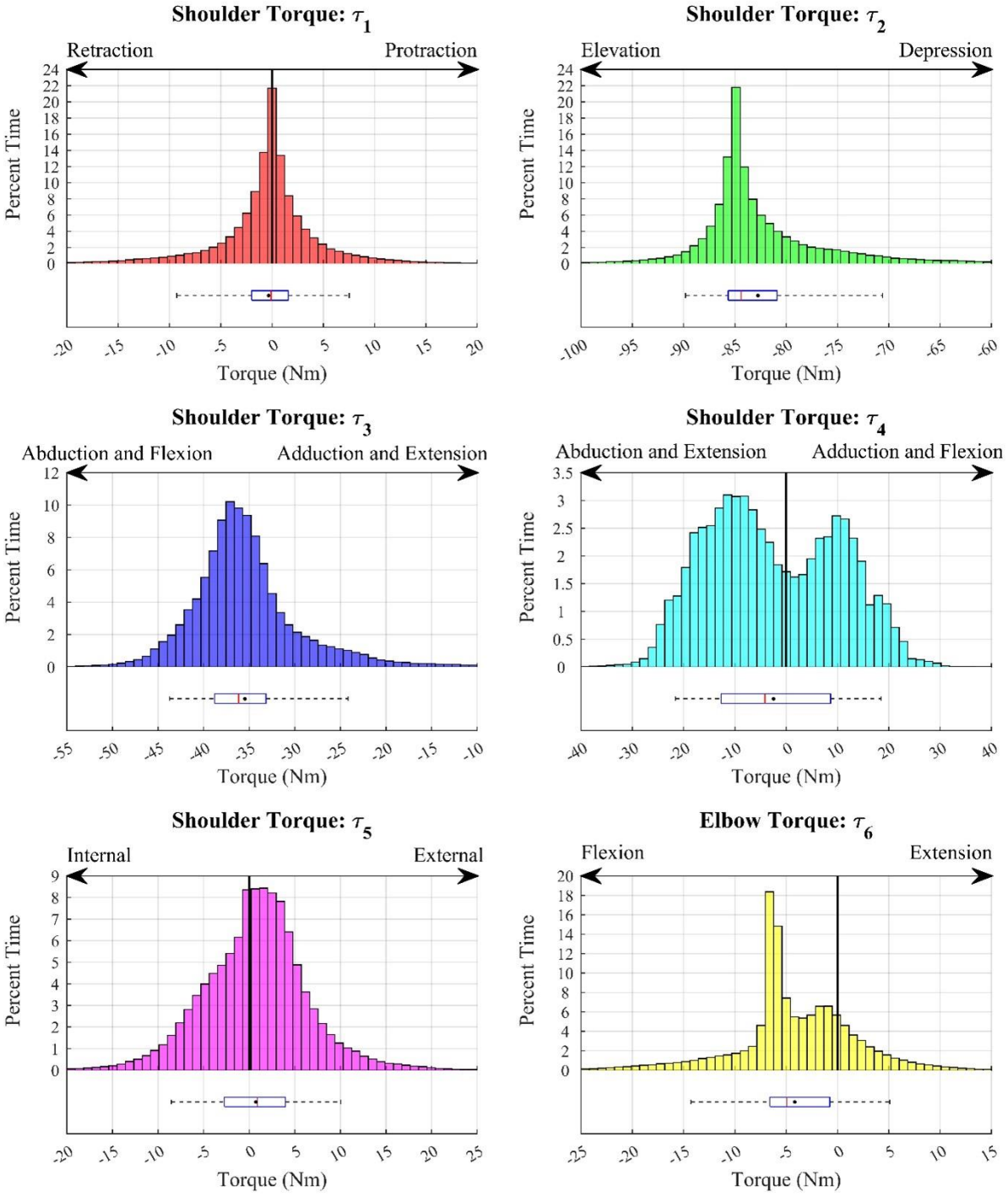

Figure 1-7 ADL analysis of joints 1-6. Graphs that result in data not centered near 0-Nm support implementing gravity balancing. Joints that benefit from gravity balancing are Joints 2 and 3 (C. Bitikofer, 2018).

This ADL analysis recommended that both joints 2 and 3 implement a gravity balance system and led to a gravity compensation design for joint 3 using constant force springs (Hill, 2019). A more complete design to gravity balance joint 2 is necessary.

1.4 Finite Element Analysis

Finite Element Analysis (FEA) is a commonly used computational approach to engineering problems. FEA is an analysis performed through the Finite Element Method (FEM). FEM is a numerical method for solving multiple partial differential equations simultaneously. The system is divided into a finite number of elements through a system discretization known as a mesh. The FEM calculates a solution through minimizing the error between elements. Typical types of FEM include structural analysis, heat transfer, fluid flow, and many others.

A FEM structural analysis of various components and systems of components in PRISM helps determine the effectiveness of the proposed design alterations and provides insight into areas of concern. All FEA results presented are performed through SolidWorks. SolidWorks FEA has the capabilities to analyze the designs while also serving as the sole design software.

1.5 Overview

This thesis will cover the redesign of the PRISM based on current parameters. Chapter 2 will cover a new gravity compensation design. This includes the physical design as well as component selection. Chapter 3 entails the altered mechanical design of PRISM. Component alterations will be presented and evaluated. Chapter 4 will review the entire design. This will include recommendations about future work as well as potential improvements.

Chapter 2: Gravity Compensation for Joint 2 of PRISM

Perfect gravity compensation of BLUE SABINO with PRISM Joint 2 requires precise knowledge of BLUE SABINO mass and center of mass properties; specifically, the mass of BLUE SABINO and the length of the PRISM links are required. The target compensated mass includes mass from all components located between Joint 2 and the end-effector such as links, actuators, sensors, wiring, and other components; this value is difficult to accurately obtain as designs are altered in development and not all physical components are accurately modeled. An alternative approach to perfect gravity compensation is to reduce the motor requirements for Joint 2. Following this approach, reducing motor requirements is achieved through applying a lifting force on PRISM to counteract the gravitational forces.

2.1 Methods

The spring attachment system is essential for providing reliable force to BLUE SABINO. The spring must continue to apply the necessary force throughout the range of motion of both Joints 1 and 2. Careful spring selection is essential for providing the desired force profile. This includes the type of spring as well as the spring characteristics. The spring attachment system and spring selection are dependent on each other. The spring attachment system influences the types of potential springs and spring selection influences attachment length and location. The design will occur in two steps: spring attachment and spring selection.

2.1.1 Previous Design Evaluation

A preliminary concept design for gravity compensation was implemented by a previous graduate student (Trimble, 2016). In this design, a cable and set of pulleys were located within PRISM to transmit forces between an extension spring and the output side of PRISM. The pulley arrangement helped minimize the change in length of the rope during PRISM movement. In turn, this lowered the variability in deflection of the spring to provide a more constant force. The initial design is presented in Figure 2-1.

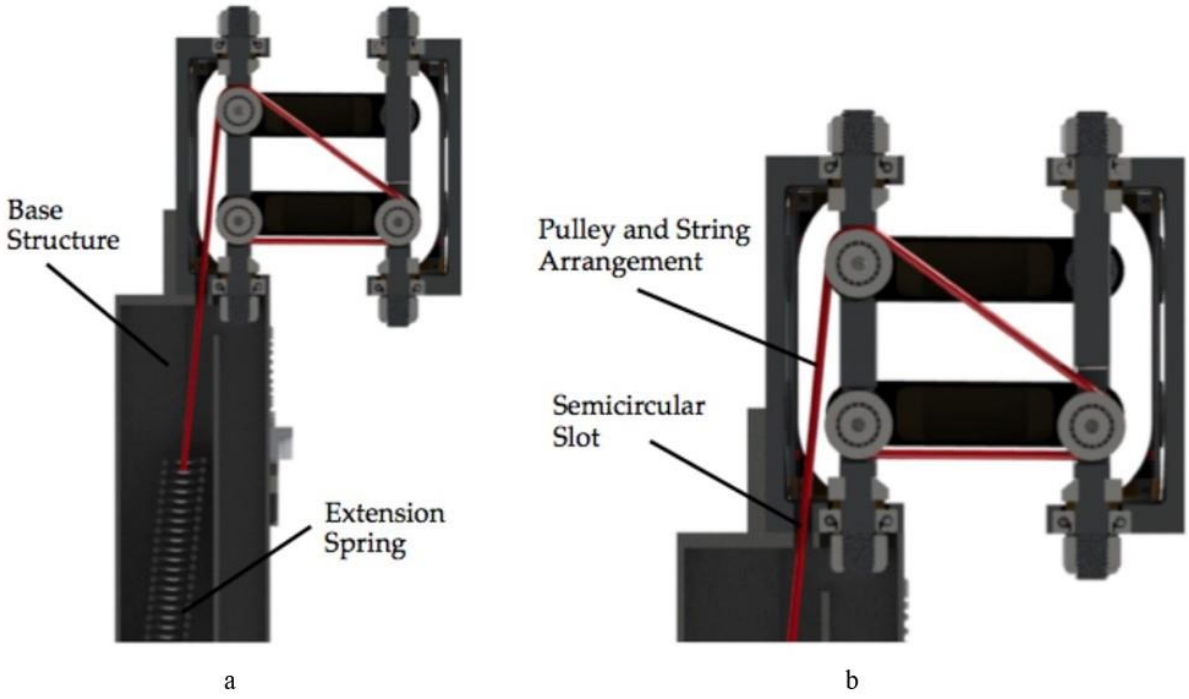

Figure 2-1 Previous spring attachment design. (a) Section view of the attachment system. The base structure that PRISM rests upon conceals the extension spring. (b) Section view of the portion of the system within PRISM. The design shows a small semicircular slot required for the rope to travel through to connect the spring and pulleys (Trimble, 2016).

While sleek in design, there were many complexities in this concept. The attachment system had no mechanical redundancy and was dependent on a singular spring and rope. It was designed to allow failure through spring deformation before catastrophic failure in the rope, increased wear on the rope in certain regions could easily change which component failed first. Each pulley added undefined frictional resistance to PRISM motion that would require compensation in the control algorithm. The gravity compensation is needed for Joint 2, but the base of the pulleys had to rotate with the movement of both Joints 1 and 2. Without the pulley rotating to follow the path of the rope, a minor risk was the rope sliding out of the pulleys completely or onto the rim of the pulley, increasing wear in the rope. The base of the pulleys had to permit enough base rotation to allow for Joint 1 alignment but limit the range of motion of the pulleys to prevent complete rotation and the rope falling out of the pulleys. The rope traveled at an angle through a narrow slot between the spring and the pulleys. The base attachment of the spring and location of the slot had to be precise to prevent wear in the rope from the slot. The design of the base tower has also changed since this first concept was made and no longer allows for internal placement of the spring.

The key mechanical component in the entire gravity balancing system is the spring. Careful selection of the spring is essential for providing the correct amount of force to PRISM. This works hand in hand with the attachment system. The design of the attachment system directly correlates to the direction and quantity of force exhibited by the spring as well as the type of springs that are functional in the system, but little research into the spring selection has been presented. The processes for a new attachment system design and spring selection will be described in detail in the following sections.

2.1.2 Design Requirements

The spring attachment system has specific design requirements for effective implementation within BLUE SABINO. The system should provide appropriate force to lower the required torque for Joint 2. It is necessary that the resulting torque requirements are within the range of the corresponding actuator. The spring attachment system should not interfere with current actuators. This includes maintaining the location of all actuators and preventing any collisions with actuators. It should also be ergonomic. The design should have a low profile and withstand transportation. The last design requirement is an improvement in safety to the entire exoskeleton. In summary, the key design requirements are Joint 2 torque reduction, maintained actuator placement, ergonomics, and improved safety. The details of these requirements are discussed in the following paragraphs.

Torque Reduction: The spring compensation must allow the actuator to support Joint 2. A previous dynamic analysis of BLUE SABINO evaluated the exoskeleton during activities-of-daily-living (ADL) without any gravity assistance elements. The minimum and maximum torque requirements for Joint 2 in this study are -60 Nm and -100 Nm, respectively, with 90% of motion requiring between -71 Nm and -90 Nm. Current estimates of BLUE SABINO in a static state establish a required torque of -60 Nm. The original actuator for Joint 2 was a SHA-20A-51 from Harmonic Drive that has a continuous torque of 21 Nm and a maximum torque of 73 Nm. This actuator could account for both static and dynamic states torque estimates with a constant -80 Nm of gravity compensation. This leaves little room for error in the gravity compensation and two large problems. First, it is difficult to achieve a simple, constant-force gravity compensation on an unbuilt, dynamic portion of an exoskeleton. Constant force springs apply low amounts of force. A potential design incorporating constant

force springs would need a large quantity of constant force springs that creates other complications, such as spring space and spring attachment. Any change in length of a linear spring will result in a change in force in the system rather than a constant force. Second, this target torque is based on an ADL kinematic and dynamic analysis. Any inaccuracies in the model could result in torque requirements beyond the actuator capabilities. A larger actuator provides a larger continuous torque and maximum torque limits, and thus provides more adjustability in design. This is a favorable characteristic in a design that is not yet manufactured. An actuator upgrade to a SHA-25A-81 with a continuous torque of 67 Nm and a maximum torque of 178 Nm provides much more flexibility in design. A summary of actuator capabilities is provided in Table 2-1.

Table 2-1 Actuator torque properties. The maximum and continuous torque limits for two Harmonic Drive actuators are compared. Continuous torque limits set design limits while the actuator can reach maximum torque outputs for shorter periods of time.

Actuator Data		
Design Model:	**Maximum Torque (Nm):**	**Continuous Torque (Nm):**
SHA-20A-51	73	21
SHA-25A-81	178	67

Maintain Actuator Placement: The development of BLUE SABINO has included critical and precise actuator placement. Kinematic and dynamic analyses of the exoskeleton were based upon these placements. Key parts of these analyses incorporate the location and mass of the actuators and links. This includes the actuators and links for PRISM. The actuators are located to support both Joint 1 and 2 movement, and key link dimensions are solidified to best follow the motions of a human shoulder. It is beneficial to limit interference from the gravity compensation system with these key actuators and links. The gravity balance system also must be anchored to a stationary component. This combination of characteristics reduces the space to fit the gravity balance system. The gravity balance system also should not restrict movement of PRISM or create a collision point with the PRISM actuators that extend beneath and behind PRISM. These actuators are circled in Figure 2-2.

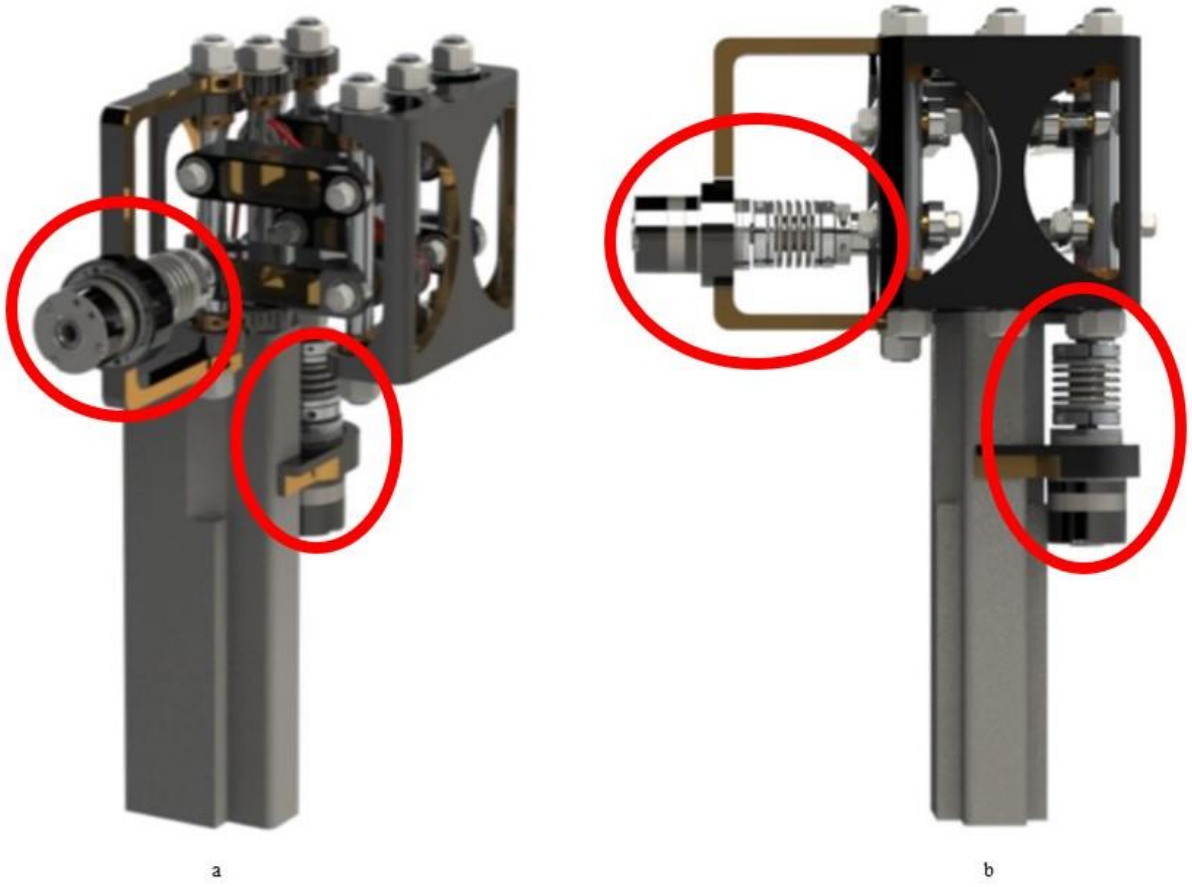

Figure 2-2 PRISM actuator locations. (a) An isometric view of PRISM. (b) A front view of PRISM. The actuators for Joints 1 and 2 are circled. These actuators are essential for providing torque to BLUE SABINO. Adapted from (Trimble, 2016).

Ergonomics: Another important design criteria is ergonomics. The gravity balance design should fit in a small space to minimize the footprint of BLUE SABINO. BLUE SABINO will have a large profile upon completion because several joints in the 30-DOF exoskeleton include remote centers, and the exoskeleton requires large supporting base structures and server racks. The exoskeleton has only continued to grow through development which results in a more awkward interface for the clinician, operator, and researchers. A smaller gravity compensation spring design results in a small profile which also assists in maintaining the range of motion of the exoskeleton. The entire exoskeleton must withstand transportation. The exoskeleton will be relocated between clinical hospitals and development areas at the university. A smaller design assists with ease of transportation, but the design itself must withstand transportation.

Safety: The primary goal of gravity assistance is safety. While the other parameters are important, safety is the top concern. A passive gravity balance system increases safety to the entire exoskeleton by reducing the load. This also reduces strain on other existing implemented safety features, such as physical hard stops, software stops, and motor brakes. While only a perfect passively gravity-balanced system can eliminate these forces, the implemented design will greatly reduce these forces. The design should also incorporate mechanical redundancy in its safety implementation, so the entire gravity assistance system is dependent on more than one component.

2.1.3 Extension Spring

A common type of mechanical spring is a linear extension spring. Every linear extension spring is designed, as the description suggests, for spring extension. The increase in length of the spring creates a force within the spring to oppose the extension. Careful consideration is important in spring selection. It is essential that the spring is compatible with the attachment system. The spring needs to both fit within the attachment system and provide the correct support to PRISM as all joints in BLUE SABINO move. Springs have characteristics unique to each spring. These characteristics define the physical size of the spring as well as the resultant force when the spring is stretched. An image including dimensions describing physical is shown in Figure 2-3.

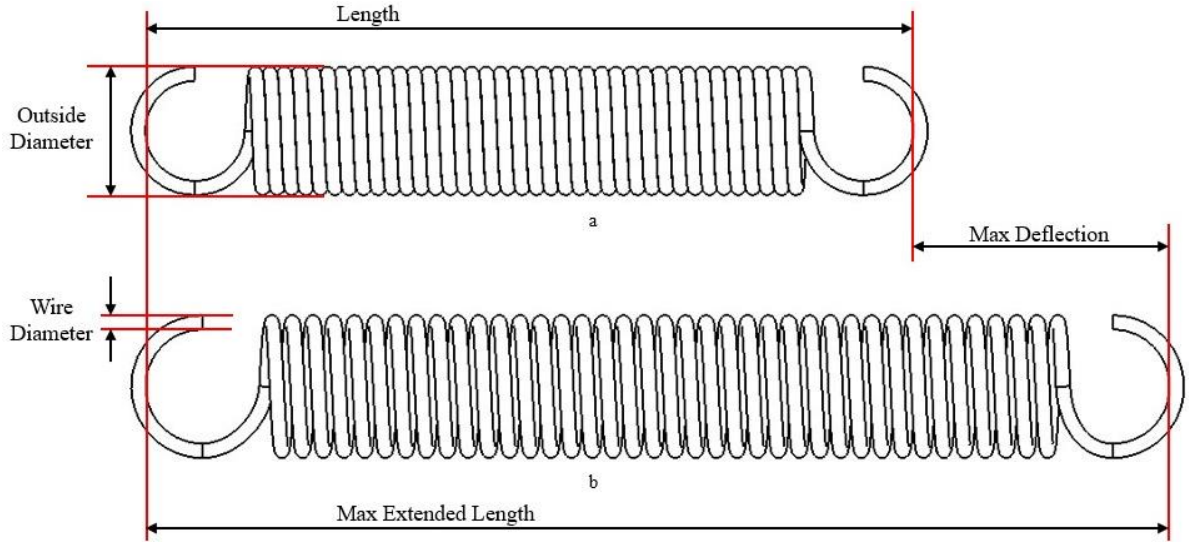

Figure 2-3 (a) An unstretched extension spring. (b) An extension spring at maximum deflection. Length is unstretched spring length. Max extended length is the length of the entire spring when fully stretched. Max deflection is the change in the length between fully stretched and unstretched. Outside diameter is the exterior diameter of the spring coils. Wire diameter is the diameter of the spring wire composing the spring.

Characteristics reported by manufacturers include material, wire diameter, outside diameter, length, spring rate, initial tension, max deflection, max extended length, and max load. Material is the substance of the spring. It is common for springs to be manufactured from stainless steel or music wire. Wire diameter is the diameter of the wire in the spring coils. The outside diameter of the spring is the distance across the outside of the coils which can directly affect collisions with other components. Altering the material, wire diameter, and outside diameter all alter the spring constant. The spring constant represents the force generated in the spring over a distance. Length, also known as free length, is the distance from end-to-end before the spring is stretched. Max deflection is the maximum distance the spring stretches before plastically deforming. Max extended length is the length of the spring when it is fully stretched. The initial tension is the force the spring withholds before stretching. Max load is the total force the spring can support when fully stretched. There are other unique characteristics that contribute to reported characteristics but are not reported themselves such as the number of coils in the spring.

2.2 Results

The two-part design of the attachment design and spring selection is presented in the following section. This includes attachment design and incorporation within PRISM. The process for selecting a spring is also presented.

2.2.1 Design Overview

The gravity compensation mechanism attaches to the support base and BLUE SABINO part 2004 as seen in Figure 2-4. The attachment surface of the support structure includes a repeating bolt pattern to allow for further modifications. Adjacent 1030 (1” by 3” by 12”) extruded aluminum profiles provided by 80/20 are bolted to the support base. Custom attachment pieces with eyebolts for spring attachment are connected to the 8020 and part 2004. Each piece holds five eyebolts for the implementation of five separate springs.

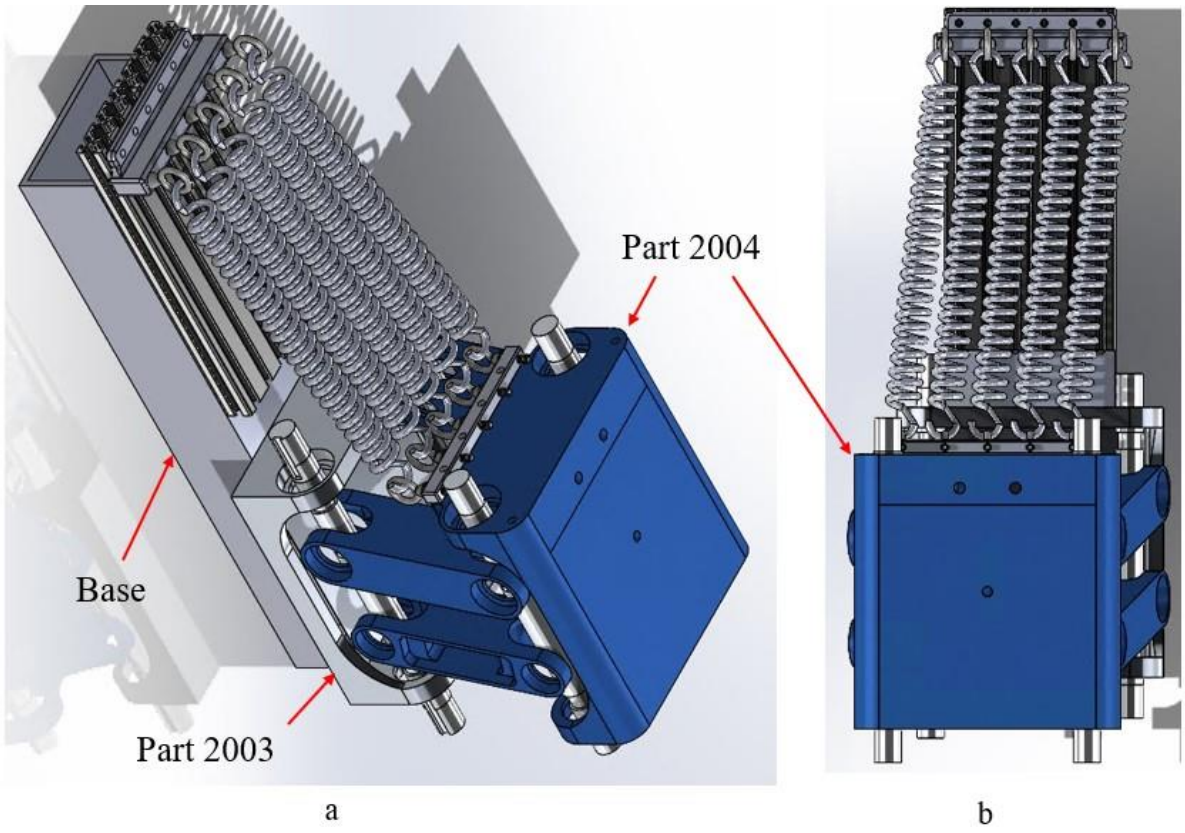

Figure 2-4 Spring attachment system design. (a) An isometric view of the design. (b) A front view of the design. The spring attachment system connects the base of BLUE SABINO with part 2004. The design includes five identical springs. These springs are intentionally close together to reduce the profile of the spring attachment system. Hardware components have been excluded from this image.

2.2.2 Spring Selection

The attachment design results in only one viable type of spring, an extension spring. Seven spring manufacturers and providers have been considered but were quickly reduced to six manufactures (Grainger was removed due to a lack of necessary information regarding spring characteristics). These manufacturers are Century Spring, Lee Spring, Acxess Spring (through TheSpringStore), W.B. Jones Spring Co. Inc. (W.B. Jones), Associated Spring Raymond (AS Raymond), and MISUMI. This totals 20,309 springs across the six providers, most of which are not legitimate options because of limitations set in the design and target torque. These limitations are based on the characteristics of outside diameter, maximum allowable force, spring length, maximum deflection, and spring rate.

Each spring has potential to collide with other springs and links within PRISM through the rotation of Joints 1 and 2. To prevent these collisions, the max allowable

diameter of the spring is limited to 1-1/4” and the actuators must remain within the 15-deg limits. These collisions can be seen in Figure 2-5.

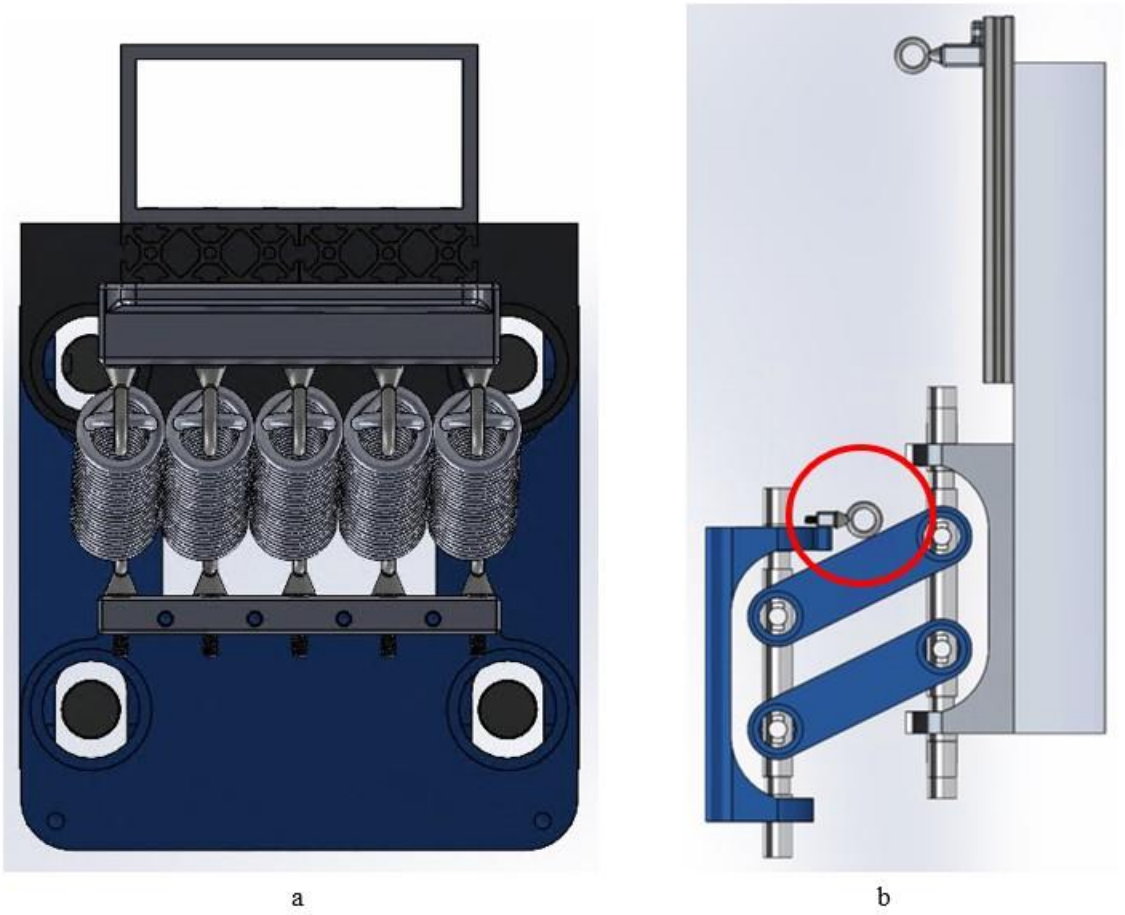

Figure 2-5 Spring collisions. (a) Springs colliding when outside diameter is 1-3/8” without Joint 1 actuation. The space between springs decreases as Joint 1 actuates. (b) Spring attachment eyebolt colliding with links as Joint 2 actuation exceeds 25-deg.

Total target force in the gravity compensation system is based on the target torque and the moment arm of the PRISM links. The resulting target force is 85 pounds. The quantity of force provided will be a range as the spring length changes. This target force is the quantity of force while the exoskeleton is at the home position. The maximum number of springs is five with the max load in each spring set to a minimum of 25 pounds to prevent plastic deformation in the spring. All these characteristics are presented in Table 2-2.

Table 2-2 Summary of spring selection characteristics.

Spring Selection Criteria	
Spring Characteristic:	**Limitation:**
Outside Diameter (in)	Less than 1.25
Length (in)	Less than 10
Max Deflection (in)	Greater than 5
Spring Rate (lb/in)	Less than 3
Max Load (lb)	Greater than 25

The unstretched length of the spring is limited to 10” to limit the height of the attachment point. The maximum deflection is a minimum of 5”. This allows for complete range of motion through Joints 1 and 2 while also keeping the spring in a stretched state. Complete range of motion of Joint 1 results in a change of length in the spring greater than 4”. The spring constant directly correlates with the difference in force at the most and least stretched states of the spring. This value has been limited to 3 pounds per inch to keep this difference at a minimum. Only 64 springs meet these spring characteristics. This data is summarized in Table 2-3.

Table 2-3 Summary of potential springs supplied by each manufacturer before and after isolating potential springs based on design characteristics.

Potential Springs by Manufacturer/Retailer		
Manufacturer/Retailer:	**Total Springs:**	**Potential Springs:**
Century Spring	4,825	17
Lee Spring	5,399	10
Acxess Spring	4,366	26
W.B. Jones	3,972	1
AS Raymond	644	10
MISUMI	1,103	0
Total Springs:	20,309	64

A cost function has been developed to determine the best possible spring. There are two approaches to develop the cost function: a spring characteristics approach or a spring performance approach. Evaluating springs based on characteristics would compare springs based on previously mentioned features such as spring constant, initial tension, spring length, etc. The weight of each characteristic in the cost function and the desired value is based on predicted performance. The actual performance of the spring is not evaluated. Evaluating

springs based on performance would compare springs based on features such as the attachment height needed to reach the desired force and the change of force in the springs as the joints in PRISM rotate. Because the spring attachment design is complete, the spring performance can be calculated with a high degree of accuracy. A performance-based approach is utilized to generate the cost function.

The three performance-based characteristics included in the spring evaluation are the change in force of the spring throughout PRISM actuation (change in force), the spring length required to achieve the target force in the home position (spring length), and the maximum allowable force in the spring (maximum force). The performance of each attribute is normalized against the best and worst spring. The resultant range for each characteristic is 0 to 1. The direction of the normalization is reversed with two of the characteristics to establish a function that results in the highest performing spring receiving the highest score. The resultant cost function is:

$$P_i = W_C\left(1-\left(\frac{C_i-C_{min}}{C_{max}-C_{min}}\right)\right)+W_L\left(1-\left(\frac{L_i-L_{min}}{L_{max}-L_{min}}\right)\right)+W_F\left(\frac{F_i-F_{min}}{F_{max}-F_{min}}\right) \quad (2)$$

where P represents the performance of the spring, i represents the ith spring, W represents the weight of the variable within the cost function, C represents the change in force, L represents the necessary spring length, and F represents the maximum allowable force in the spring. The springs are evaluated based on three separate weighting distributions. The weighting of the three characteristics is found in Table 2-4.

Table 2-4 Cost function analysis for spring selection. The three final cost function distributions are presented below. The characteristics considered are change in force, spring length, and maximum force.

Spring Cost Function Weighting Distributions			
Trial #:	**Change in Force:**	**Spring Length:**	**Maximum Force:**
1	0.6	0.3	0.1
2	0.6	0.4	0
3	0.55	0.35	0.1

The ranking of each spring in each weighting distribution has been considered. The final spring is Spring #30, PE095-1250-45105-MW-6500-CO-N-IN provided by Acxess

Spring. The attachment height to reach 85 pounds is 15.25 inches above PRISM (specifically, above part 2003).

2.3 Discussion

The spring attachment system is designed for adjustability. The adjustability in this design is essential for allowing a variety of springs. This is a key benefit as the target force for the springs varies. It creates an avenue for simple modifications once PRISM is manufactured and evaluated. The repeating hole patterns along the base structure allow for various vertical attachment locations for the 8020 parts. The 8020 components can extend above the base structure as needed. This has both positive and negative effects. By extending the attachment height, the number of potential springs for the system is greatly increased. Limiting the attachment height to 12 inches above PRISM reduced the number of potential springs to one. Other important factors, such as the change in force as PRISM actuates, could not be included in the spring selection if there was only one potential spring. The increased height increases the profile of the total design. This is costly both functionally and visually. An increased height increases potential with collisions with other parts of BLUE SABINO. One known collision is from the 1005 sub-assembly as seen in Figure 2-6. This sub-assembly is located on the posterior side of the upper arm. An increase in size of this sub-assembly from the 4-bar development and an increase in height of the PRISM gravity balancing system have created a collision point. Physical and software stops will be required within BLUE SABINO to prevent this collision or alteration to the attachment points on either side of PRISM.

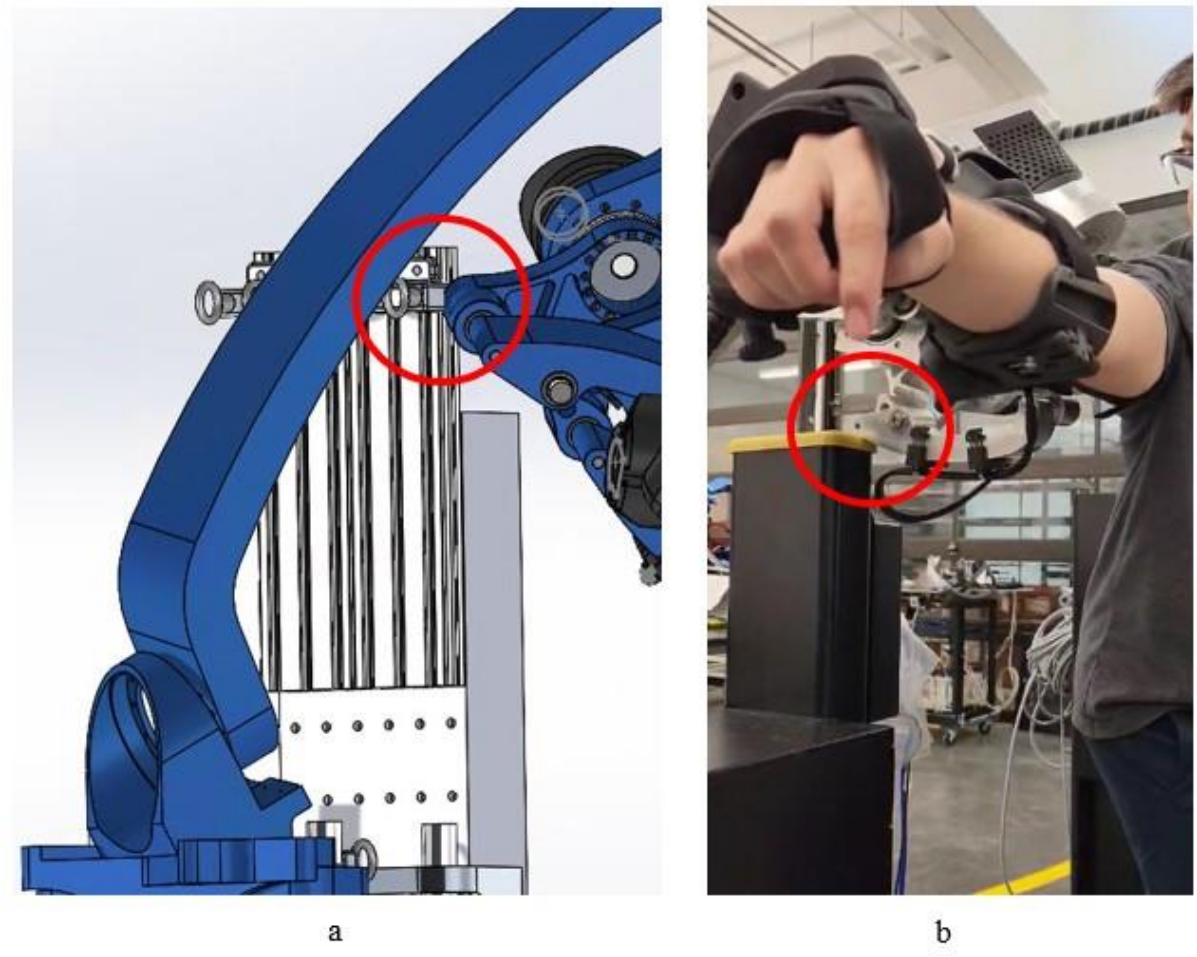

Figure 2-6 Base and 1005 sub-assembly collision. (a) The 4-bar mechanism within the 1005 sub-assembly colliding with the base in CAD. (b) A different part within the 4-bar mechanism colliding with the current base.

The design is also simple to manufacture. Most of the manufacturing work is drilling holes for bolt attachment. The components are designed for simplicity. The part with the most complex geometry is the component that connects the springs and 8020. This complexity is designed to reduce weight and limit stress concentration points but remains simple to manufacture.

The spring selection process was not just a study investigating which springs would work but rather investigating which springs would work the best. Most springs that would not work were eliminated in the selection criteria. The remaining 64 springs were evaluated through the cost function. The weightings used were based on importance within the design. The change in force in the spring as Joint 2 actuates is a measure of the gravity balancing effectiveness. A smaller change in force results in a more consistent force applied to PRISM.

This is the primary goal of the gravity compensation system and is thus the most important evaluation characteristic. The required spring length directly correlates with the attachment height and overall profile of the system. The maximum force in the spring influences the factor of safety in the spring components. Eventual physical and software stops will prevent all potential springs from overstretching or exceeding the maximum force. The maximum force is of the least significance. The order of importance for characteristics is easy to identify. The difficulty comes from evaluating the importance numerically within the cost function. This has resulted in three separate evaluation trials with varying weighting factors. The performance of the springs across all three trials. The top three springs in each trial are below in Table 2-5.

Table 2-5 Top performing springs. The four highest performing springs are compared with each cost function trial.

Top Performing Springs in Each Trial			
Spring Number:	**Ranking in Trial 1:**	**Ranking in Trial 2:**	**Ranking in Trial 3:**
28	2nd	8th	4th
29	1st	3rd	2nd
30	3rd	1st	1st
32	9th	2nd	3rd

All four of these springs are great potential options. Spring #30 was chosen due to its best collective performance. A factor not considered for this study was monetary cost. The selection is based on performance, not economics.

Another design consideration is the effect of the change in force on the actuator requirements. The goal is to reduce the needed torque in the actuators, but the amount of torque relief applied by the springs changes as Joints 1 and 2 actuate. This numerical value can be obtained through modifying the kinematics and kinetics. The derivation for this modification is found in Appendix A. Due to the attachment location of the springs, Joint 1 rotation from the home position results in torque generated from the springs in Joint 1. The torque for Joint 1 fluctuates between -3.84 Nm and 3.84 Nm throughout all orientations of PRISM. Joint 2 torque compensation fluctuates between -48.19 Nm and -61.22 Nm. In the home position, the spring does not apply torque to Joint 1 and applies -56.79 Nm of torque to Joint 2. The joint torque as the joint angle changes is presented in Figure 2-7.

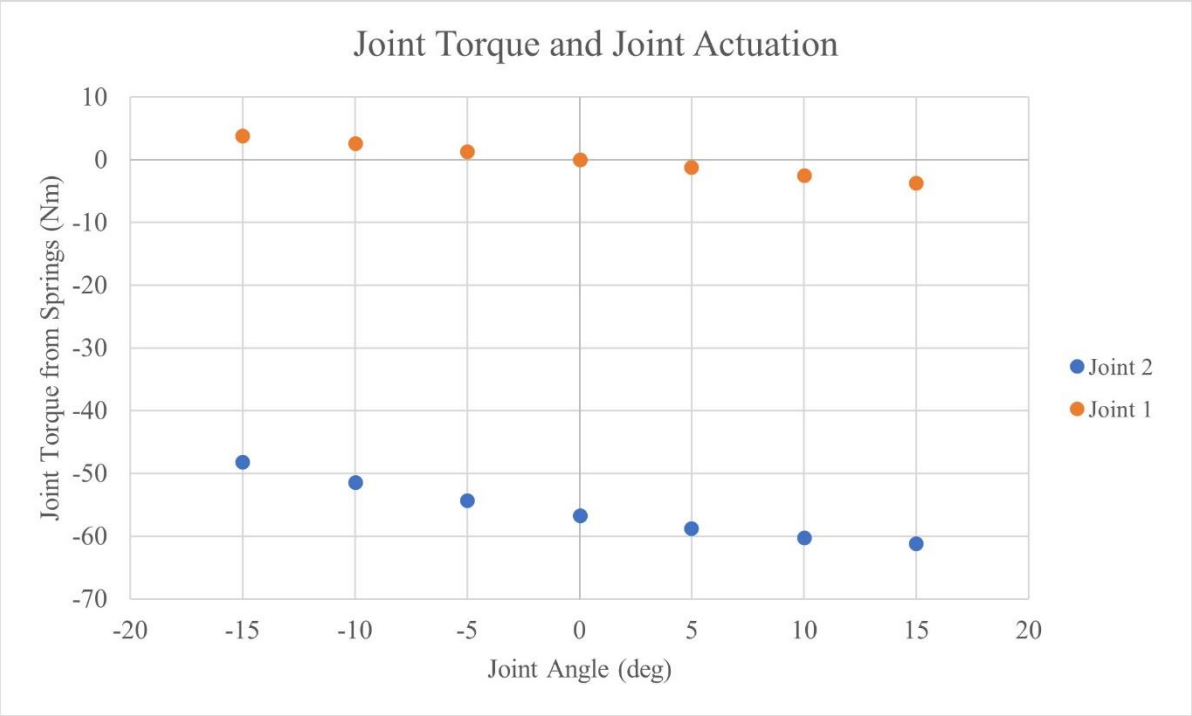

Figure 2-7 Joint torque applied from springs as the joint actuates. During joint actuation, the other joint is in the home position.

Chapter 3: Improving PRISM Design

PRISM serves two main purposes in the BLUE SABINO exoskeleton: 1) to enable scapulohumeral rhythm and 2) to support distal BLUE SABINO joints. Scapulohumeral rhythm is achieved through the design of PRISM. The links and actuators are placed to allow the shoulder girdle to move laterally and vertically. It is essential that PRISM simultaneously supports the weight of all other joints as it executes this motion. The ability of PRISM to support these links is directly correlated with the design, robustness, and strength of the system and individual components.

3.1 Design Goals

The primary stress experienced on PRISM is from supporting the rest of BLUE SABINO. The location of the distal portions of the exoskeleton relative to PRISM results in torque within the links of PRISM causing PRISM to twist. This twisting action within PRISM results in small PRISM deflections having much larger deflections at the end-effector of BLUE SABINO. A design goal of BLUE SABINO is to minimize this end-effector deflection.

PRISM is also responsible for translating the rest of the exoskeleton. The actuator for Joint 2 experiences the largest torque requirements in the exoskeleton. This torque is directly related to the weight of BLUE SABINO components. Minimizing weight within PRISM reduces actuator torque requirements. Another design goal of PRISM is to minimize the weight within PRISM. These two design goals (minimize deflection and weight) directly compete. A key part of PRISM is designing components that balance these factors.

3.2 Methods

Separate designs of components within PRISM are evaluated relative to each other. The key components evaluated are parts 2004, 2009, and 2010. These three parts are all structural components that contribute directly to the deflection and mass of PRISM while also having a high degree of variability in design. Other parts within the assembly are 2003, 2005, 2008, and 2017. These parts all contribute structurally to the design but have low variability in design. All included FEA components are shown in Figure 3-1.

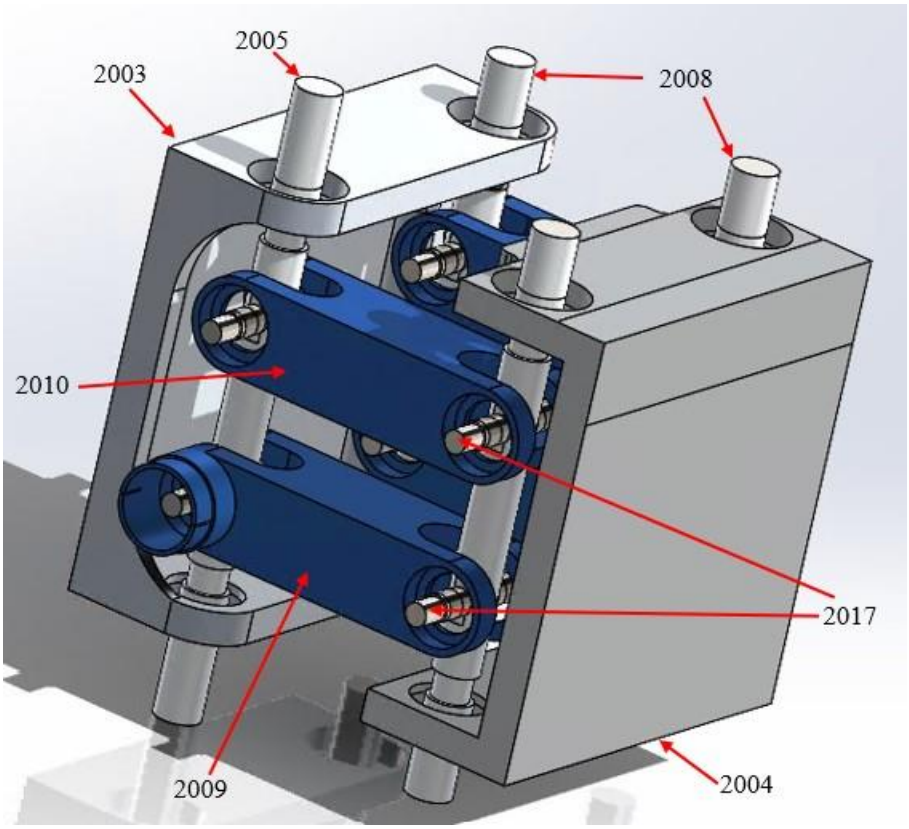

Figure 3-1 PRISM FEA setup. PRISM is set in the home position with all components labeled that are included in the FEA. There are multiple copies of parts 2008, 2010, and 2017 within the assembly.

Several of these components have had features removed in non-essential locations to improve mesh quality as seen in Figure 3-2. All other PRISM components are not included in the simulation.

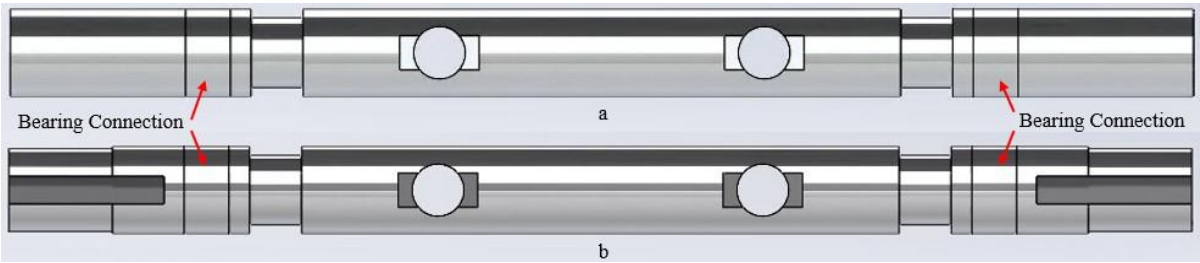

Figure 3-2 Example of modification for mesh quality. (a) Modified part 2005. (b) Actual part 2005. Both ends of part 2005 have been smoothed to increase mesh quality. This does not affect any stresses in the FEA as it is past the connection points but increases mesh quality and decreases calculation time.

All variations of parts 2004, 2009, and 2010 undergo the same static SolidWorks FEA evaluation. It is essential to establish a robust process for the evaluation to ensure consistency between simulations. Components of the analysis that must remain constant between

evaluations are connections, loads, fixtures, and meshes. Individual components within the PRISM assembly are evaluated as well as the entire assembly with hardware removed. Hardware components that contribute to deflection are also considered for modification.

3.2.1 Connections

Connections are responsible for the way different components interact within an assembly FEA. There are two types of connections: component interactions and connectors.

Component Interactions: Component interactions determine the behavior of components that contact each other. The three types of interaction are bonded, contact, and free. *Bonded* treats the components as if they are welded together within the simulation. *Contact* interactions prevent interference with components during simulation. *Free* interactions allow components to move freely and intersect each other during simulation. These component interactions are applied on a global, component, and local level with each more specific level overriding the previous level. The global contact interaction is set to contact in these simulations, but all interacting components are further defined with connections.

Connectors: Connectors are mechanisms that define how parts connect with other components in an assembly. The primary use of connectors is to replace complex components. Connectors within SolidWorks are: Rigid, Spring, Pin, Elastic Support, Bolt, Link, Edge Weld, Spot Welds, and Bearing. PRISM incorporates springs, pins, bolts, and bearings, but the only implemented connectors in FEA are the rigid connector and the bearing connector. The springs within PRISM can be modeled as forces instead of connectors because the study is static in nature, not dynamic. The pins are represented through modeled pins. Rigid connectors join the pins with the shafts to prevent the pins from sliding within the shafts. Components that are not included in simulation normally prevent this motion. The bolts are modeled with a fixture. The bearings connect a shaft face with a housing face, and corresponding shaft and housing components are incorporated in the model to enable this connector.

Rigid connectors are a common type of SolidWorks connector. It takes multiple surfaces and treats them as if they are rigid. The components are forced to move together. Rigid connectors can have negative effects on simulations as well such as high stress concentrations in incorrect locations if implemented on parts that are not supposed to move

together. The FEA performed in this study incorporates eight rigid connectors, one for each pin-shaft connection which are all featured in Figure 3-3.

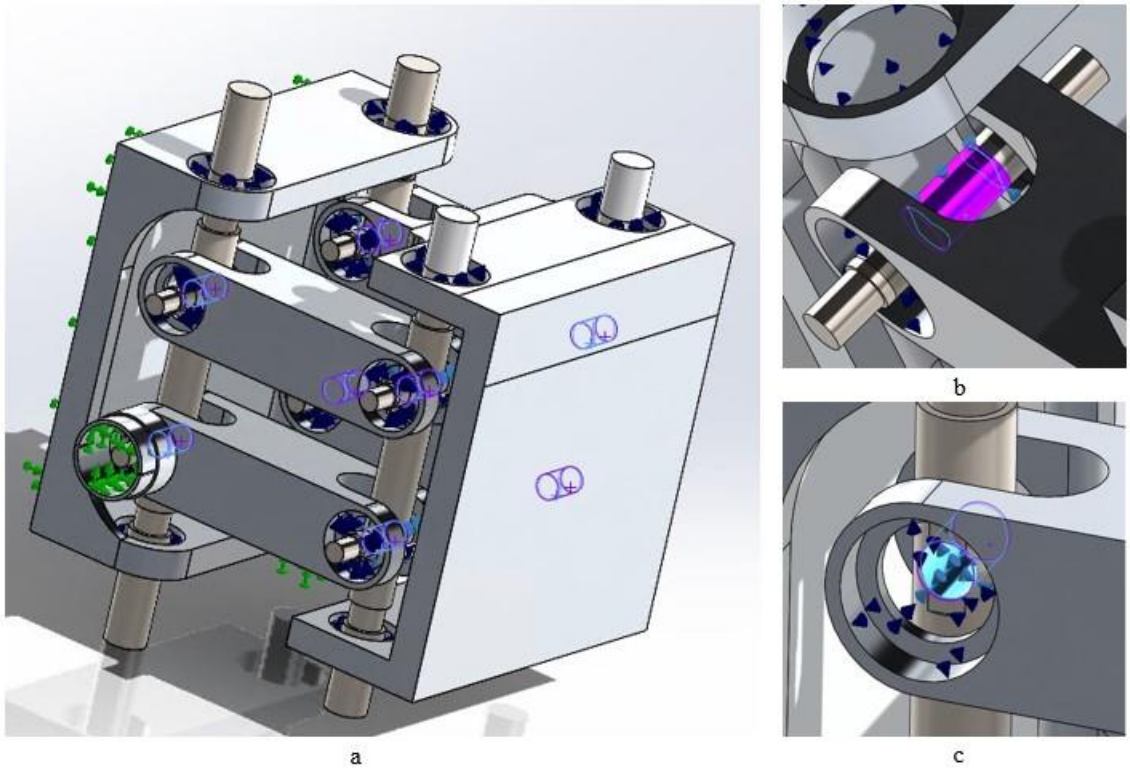

Figure 3-3 Rigid connectors. (a) An image containing all eight rigid connectors. (b) The rigid connection on the outer diameter of part 2017. (c) The rigid connection within a hole in part 2005.

Bearing connectors have three key properties: self-alignment, rigidity, and stability. *Self-alignment* allows for off-axis rotation. The inner race of the bearing deflects and rotates as the shaft off axis as it experiences loading. This feature is specifically for self-aligning bearings or ball bearings with 2 or more rows of balls within the bearing. *Rigidity* determines whether the bearing is treated as a flexible or rigid member. SolidWorks incorporates flexibility in bearings by simulating radial and axial springs between the shaft and housing. The flexible option requires the input of axial and radial stiffness values of the springs. These values are not readily available from spring manufacturers and require experimentation to collect (Branz, 2019). *Stability* prevents the shaft from rotating freely about its axis by integrating low torsion springs to prevent continuous rotation. The FEA performed in this study does not allow self-alignment because the physical bearings are tapered-roller bearings and do not allow for off axis rotation. It assumes rigid bearings due to a lack of flexibility properties, and it does not stabilize shaft rotation for all bearing connectors due to fixtures

and mechanical restraints preventing continuous rotation. All 24 bearing connectors with these properties are illustrated in Figure 3-4.

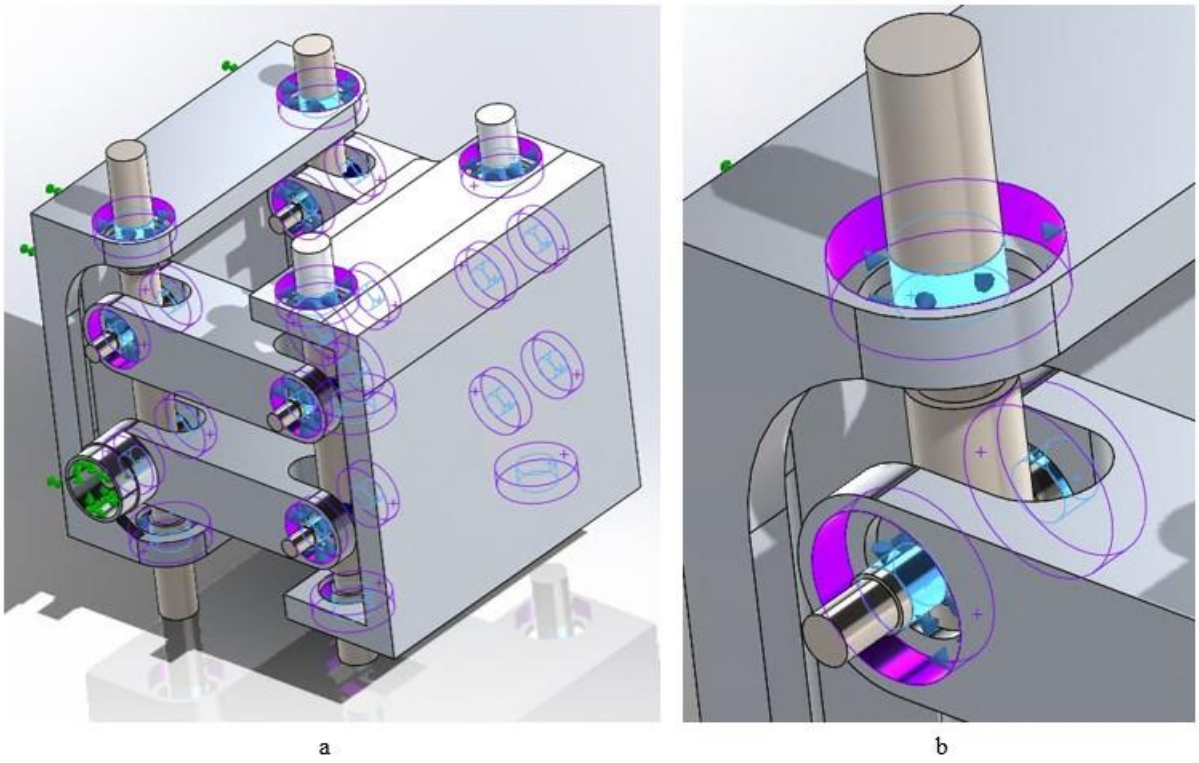

Figure 3-4 Bearing connectors. (a) The 24 bearing connectors within the FEA. (b) A close-up of three bearing connections.

3.2.2 Loads

There is one loading condition considered in multiple poses for the FEA. The loading condition is a worst-case loading conditions in two separate poses. The theorized worst-case loading condition occurs when PRISM is supporting weight of BLUE SABINO, the arm weight of an individual in the exoskeleton, and the weight of an individual that falls on the end-effector of BLUE SABINO all while the end-effector is fully extended from PRISM and the spring mechanism is not supporting PRISM. Initially, three BLUE SABINO fully extended configurations were considered for loading conditions: across the body (90-deg shoulder flexion and 45-deg horizontal adduction), in front of the body (90-deg shoulder flexion), and away from the body to the side (90-deg shoulder abduction). The configuration of the arm extended away from the body to the side was excluded due to this configuration resulting in BLUE SABINO center-of-mass and end-effector locations much closer to PRISM than the other two configurations, and, thus, significantly lower stresses and

deflection. A 95th-percentile man weighs 98.5 kg with the upper arm, lower arm, and hand weighing 2.5 kg, 1.72 kg, and 0.61 kg respectively (National Aeronautics and Space Administration, 1995). The resulting forces are 312 N (from weight of BLUE SABINO, not including PRISM or hand DOFs), 25 N (from weight of operator upper arm), 17 N (from weight of operator lower arm), and 1000 N (from weight of operator hand, weight of hand portion of exoskeleton, and weight of 95th-percentile male). These forces are represented as four separate remote loads. The locations of these forces were collected through CAD evaluation and are presented in Table 3-1.

Table 3-1 FEA Remote Loads. The locations and magnitude of each remote load. Each location is based upon a coordinate frame with an origin (0,0,0) established on part 2004. The positive direction of each axis is: x-axis extends towards operator midline, y-axis extends above operator, z-axis extends in front of operator.

FEA Remote Load Locations and Magnitude				
Pose:	**BLUE SABINO 5-DOF: (x, y, z) mm**	**Upper Arm: (x, y, z) mm**	**Lower Arm: (x, y, z) mm**	**Hand: (x, y, z) mm**
1	(241, 349, 302)	(501, 338, 400)	(501, 351, 607)	(713, 356, 514)
2	(340, 262, 348)	(529, 350, 378)	(713, 356, 514)	(988,390, 712)
Force	312 N	25 N	17 N	1000 N

3.2.3 Fixtures

Fixtures restrain movement and deflection on an applied vertex, edge, or surface of a modeled part. The fixture prevents deflection in the selected body but not the entire part. They are essential for structural analysis in FEA, as they prevent applied forces and loads from causing dynamic motion. Fixtures are applied frequently on surfaces that mechanically prevent motion, such as a bolted connection plate. There are three fixtures within the PRISM simulation. One fixture represents attachment to the base structure, and the other two fixtures represent motor faces that allow and prevent movement. An analysis without motor fixtures should result in PRISM falling as bearings do not inhibit motion.

3.2.4 Mesh

FEA is a numerical technique to solve complex problems by separating the model into smaller portions. These smaller pieces are known as elements, and they connect at nodes. The mesh is the resultant geometry from the creation of the smaller pieces. Variance within different meshes results in a significant difference within the FEA through variation in

element size. A finer mesh increases the accuracy of simulation results but also increases simulation time. Many types of software that perform FEA require the operator to build the mesh, but SolidWorks automatically creates a mesh with user-defined guidelines. This allows for quicker mesh creation but can create inaccurate meshes.

SolidWorks provides three separate meshing techniques and the ability to alter the mesh density in each technique. The three meshing techniques are standard mesh, curvature-based mesh, and blended curvature-based mesh. Standard meshing uses the Voronoi-Delaunay meshing scheme (Meshing Options – 2023 – SOLIDWORKS Help, 2023). In this scheme, the global size and tolerance of the mesh are specified, and there is an option for automatic mesh control around small features. Curvature-based meshing creates more elements near areas with high curvature. This greatly increases the mesh quality because locations with curvature generally are the location of stress concentration points. Blended curvature-based meshing is a more advanced technique for creating a smoother mesh as the transitions between curvature occur (Meshing Options – 2023 – SOLIDWORKS Help, 2023). Both curvature-based approaches specify the maximum element size, minimum element size, minimum number of elements in a circle, and element growth size ratio. All meshing techniques can also specify the Jacobian points which is the number of points used to evaluate the distortion level of the elements. The mesh quality can be improved by altering the characteristics in each meshing technique directly or by utilizing a slider bar that provides a general mesh measure of “course” and “fine”. SolidWorks also has a mesh control feature. It allows for specific mesh quality around specified surfaces.

The mesh is created in all simulations with the blended curvature-based approach. The maximum element size is 20-mm while the minimum element size is 1-mm. The minimum number of elements in a circle, element growth size ratio, and Jacobian points are unaltered (8, 1.4, and 16 respectively). There is also mesh control around every rigid and bearing connection with a maximum element size of 5-mm and a minimum element size of 4.5-mm. Figure 3-5 includes an example mesh with these characteristics.

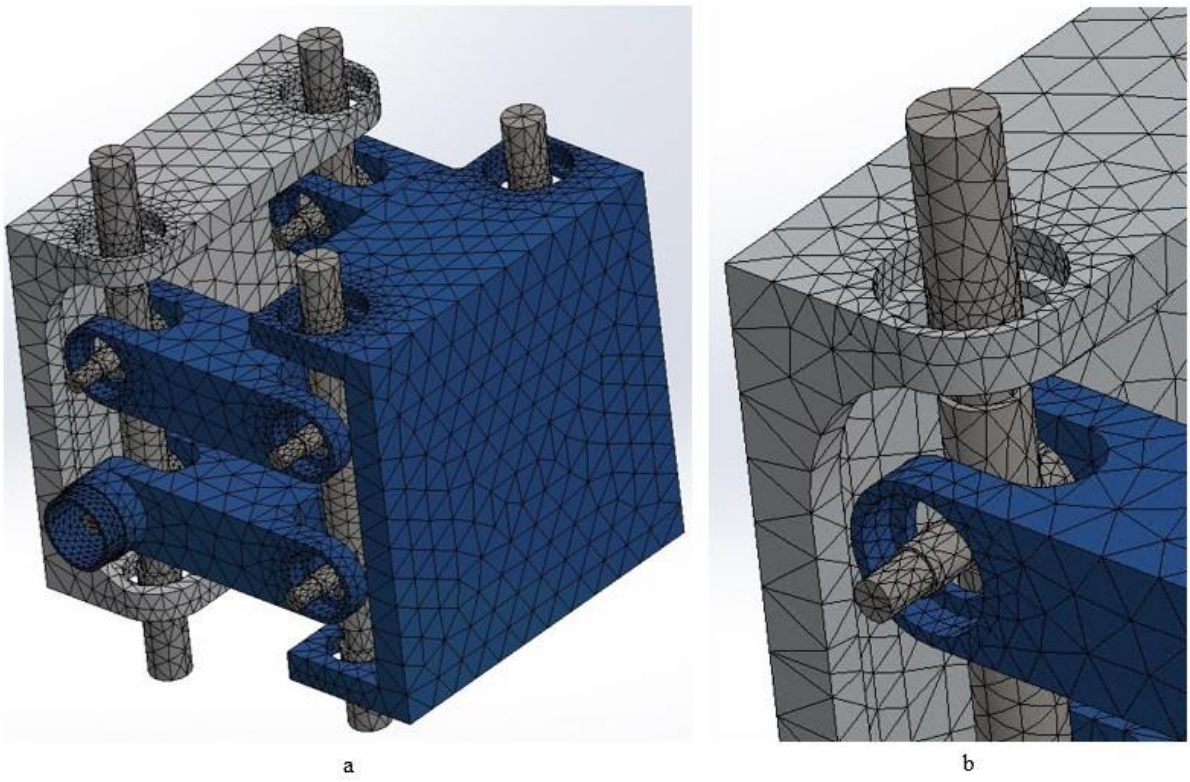

Figure 3-5 Mesh of PRISM. (a) Entire mesh of PRISM. (b) Close up on part of the mesh. The mesh transitions from coarser to finer around mesh control and curved surfaces.

The quality of an automatically generated mesh involving multiple parts is difficult to understand intuitively. There is a generic slider that SolidWorks provides to determine whether the mesh is fine or course. This slider does not communicate the details of mesh accuracy but only a general measure of "fineness". One way to evaluate mesh performance is through the aspect ratio. SolidWorks meshing creates elements that are tetrahedrons. The aspect ratio is the ratio between the largest normal and shortest normal in the tetrahedron. An aspect ratio of one is the smallest possible aspect ratio and communicates a tetrahedron that has four surfaces of the same shape and size. A large aspect ratio communicates a tetrahedron that has one or more surfaces that varies in shape and/or size. In general, a lower aspect ratio increases the accuracy of the stress calculation within that element as well as the elements around it. SolidWorks calculates the aspect ratio for every element created during the meshing process. The aspect ratio of the part or assembly is summarized through three metrics: maximum aspect ratio, percentage of elements with aspect ratio less than 3, and percentage of elements with aspect ratio greater than 10. Guidelines for a good mesh include the maximum aspect ratio between 10 and 20, the percentage of elements with aspect ratio

less than 3 above 90%, and the percentage of elements with aspect ratio greater than 10 as low as possible (Petrock, 2020). A “fine” mesh does not necessarily correlate with these aspect ratio parameters as shown in Figure 3-6.

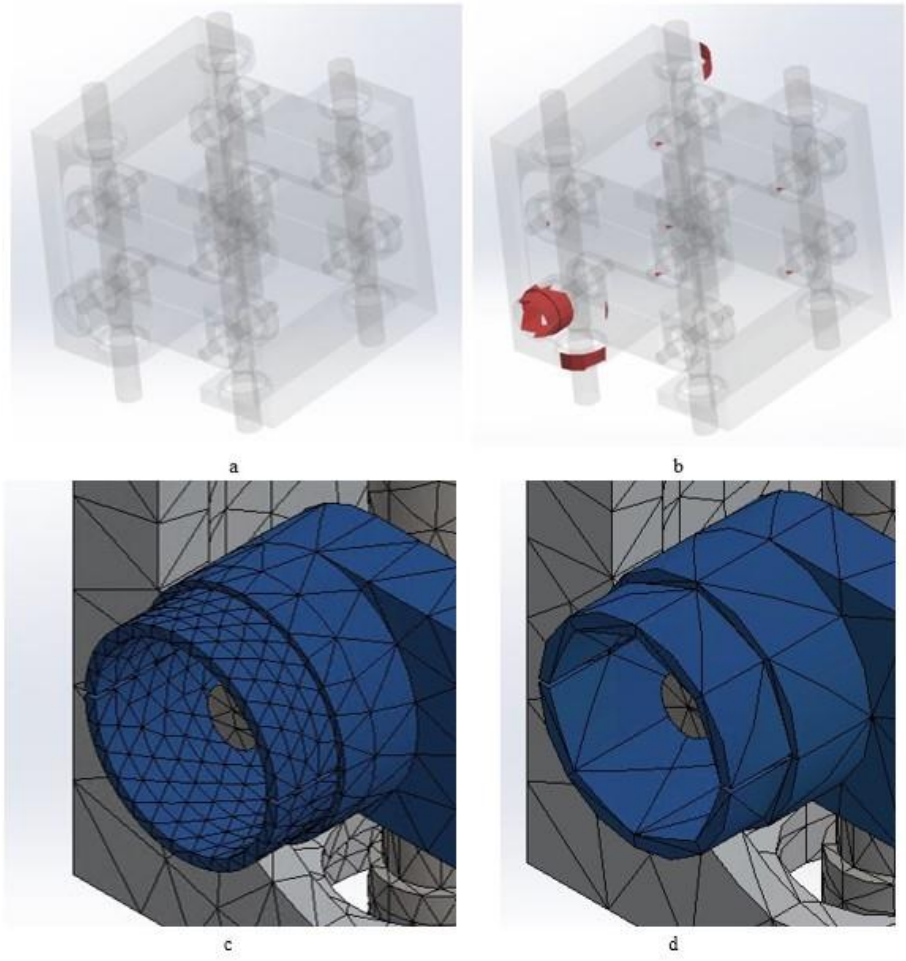

Figure 3-6 Aspect ratio and mesh of two separate mesh conditions. (a) The aspect ratio of a mesh with mesh control but the slider not at max “fineness”. (b) The aspect ratio of a mesh without mesh control but the slider at max “fineness”. All other mesh aspects have been held constant. The red elements have an aspect ratio that is greater than 10. (c) Mesh on part 2009 with the same mesh control as (a). (d) Mesh on part 2009 with same mesh conditions as (b). the difference in mesh density is visibly noticeable between (c) and (d).

3.2.5 Hardware Modification

One solution to minimizing deflection is altering the hardware within PRISM. Previous studies on the 1005 sub-assembly in BLUE SABINO have demonstrated that most of the deflection happens within the ball bearings (Branz, 2019). This is where most of the deflection is expected within PRISM as well. PRISM has more bearings than the 1005 sub-assembly and experiences higher loads. Each side of PRISM contains 24 bearings. All the

bearings in BLUE SABINO have been implemented or modeled as ball bearings. One potential way to decrease deflection is to alter the ball bearings within PRISM.

Ball bearings are not known for a high resistance to deflection. The principle behind the underperformance is based on the functionality of ball bearings. The balls within the bearing translate force between the inner race and outer race of the bearing. Because the balls are spherical in shape, the contact point that transfers the force between the ball and other components is a point contact. This results in higher stress and greater deformation. One way to improve stiffness in a bearing is to increase the amount of contact surface within the bearing. Most ball bearings are also only designed to support radial loads which is not the loading condition for every bearing within PRISM.

Tapered-roller bearings provide greater stiffness than ball bearings. This is based on how tapered-roller bearings function. The motion in tapered-roller bearings occurs as cylinders rotate in the bearings. The cylinders transfer forces between components in the bearing. The contact surface area is the length of the cylinder. This is a significant improvement to the point load that the balls in ball bearings undergo and is a large reason why tapered-roller bearings have higher stiffness than ball bearings (Schaeffler Group USA, n.d.). Tapered-roller bearings are also frequently designed to withstand radial and thrust loadings. There are many other factors that contribute to the stiffness in a bearing. While tapered-roller bearings are generally stiffer, it is not guaranteed that every tapered-roller bearing is stiffer than every ball bearing. Manufacturing quality, size of the bearing, rated load, and the loading experienced by the bearing are all additional potential factors that can affect bearing stiffness.

The only hardware modification to improve stiffness in PRISM is the replacement of ball bearings with tapered-roller bearings. All 24 bearings have been transitioned to tapered-roller bearings. There are two separate sizes of bearings. The 16 ball bearings within the input (part 2009) and floating links (part 2010) originally had an inner diameter of 15-mm, an outer diameter of 35-mm, and a thickness of 11-mm. Each bearing was replaced with a tapered-roller bearing with an inner diameter of 15-mm, an outer diameter of 42-mm, and a thickness of 11-mm. The size of both links was increased in size to accommodate the larger

bearings. There is an offset between inner race and outer race contact surfaces that is not present in ball bearings. Figure 3-7 depicts this offset.

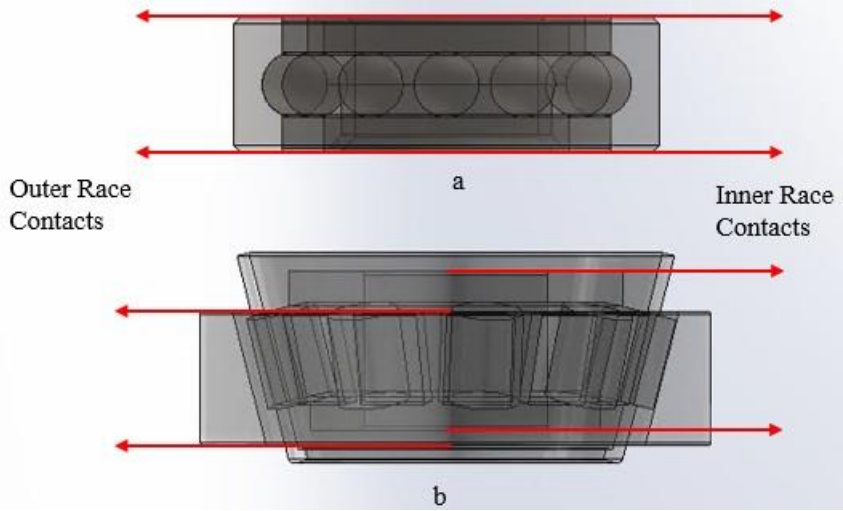

Figure 3-7 Example of replacing ball bearings with tapered-roller bearings. (a) Previous ball bearings with aligned contacts of the inner and outer races. (b) Tapered-roller bearing with contact offsets between the inner and outer race. The part replacement results in spacer and part modificaiton.

The eight ball bearings located in the ground and output links (parts 2003 and 2004) originally had an inner diameter of 25-mm, an outer diameter of 52-mm, and a thickness of 15-mm. Each bearing was replaced with a tapered-roller bearing that has an inner diameter of 25-mm, an outer diameter of 52-mm, and a thickness of 13-mm. The housing for the bearings in the c-shaped ground and output links was decreased to accommodate the smaller bearing. The four links were not the only parts affected by changing the bearings. The spacers, pins (part 2017), and vertical rods (parts 2005 and 2008) also needed modification due to the bearing alteration.

3.3 Results

The three parts altered between simulations are the output link (part 2004), input link (part 2009), and floating links (part 2010). The simulations are split into three categories based upon which component was modified. Each design is analyzed in two poses. The results of both stress and displacement are important for establishing logical FEA results, but the key measurements are mass (measured within SolidWorks) and displacement. An example of FEA results for a single design are shown in Figure 3-8.

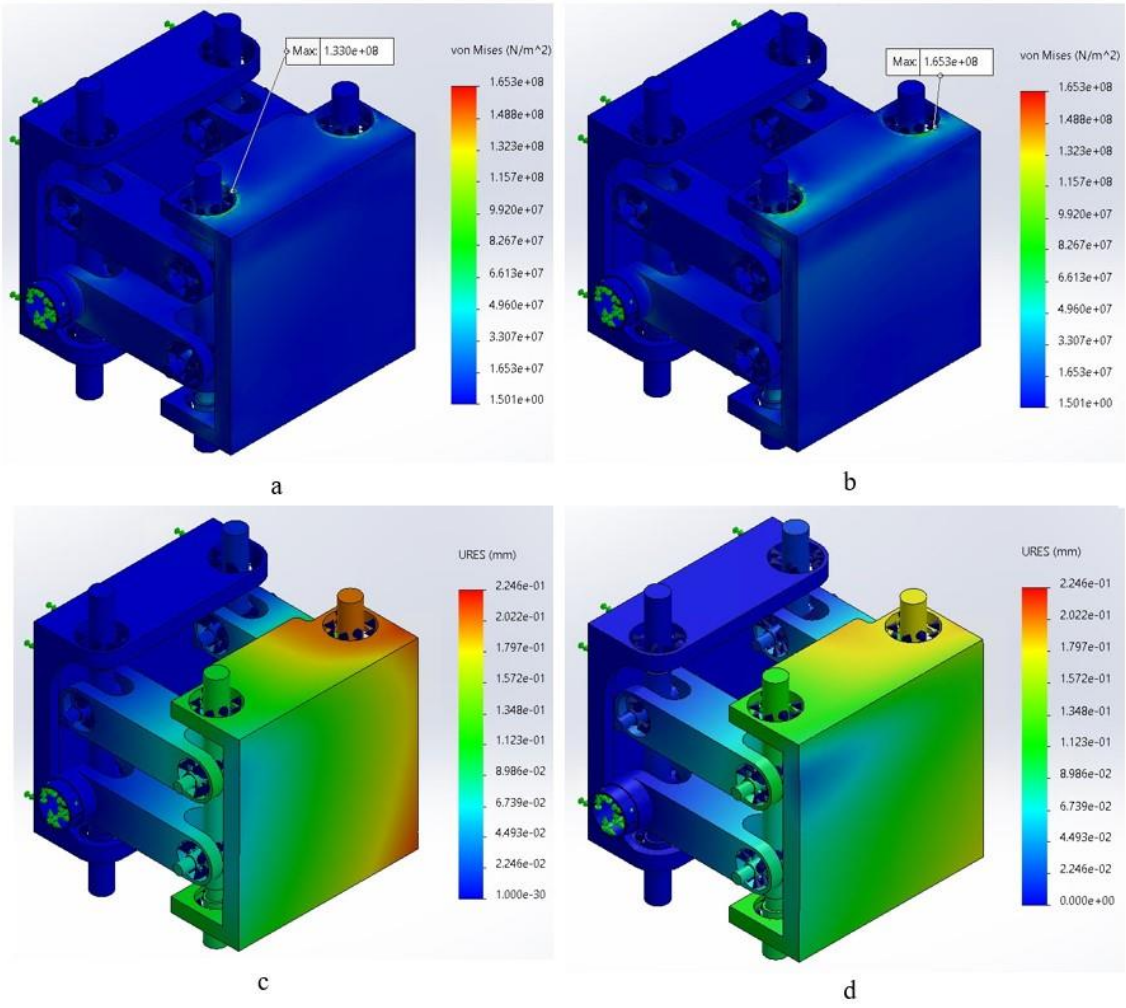

Figure 3-8 Example of an FEA. (a) Stress plot for pose 1 with maximum stress at posterior-superior bearing on part 2004. (b) Stress plot for pose 2 with maximum stress at anterior-superior bearing on part 2004. (c) Deflection plot for pose 1. (d) Deflection plot for pose 2.

3.3.1 Part 2004 Simulations

The first part analyzed is the output link. Input and floating links were kept in a constant state for all the trials. The percentage of mass reduction and the percentage of displacement reduction for every design is shown in Figure 3-9. The percentage of mass reduction is calculated from the solid component without any material removed. The percentage of deflection is calculated from the design variation that causes the most deflection in the assembly, not deflection in the individual component. The data trends from the top left to the bottom right. This is the expected trend as more mass correlates with higher stiffness and less deflection. Ideally, there would be a design in the top right corner of the graph, maximizing the reduction in both mass and deflection.

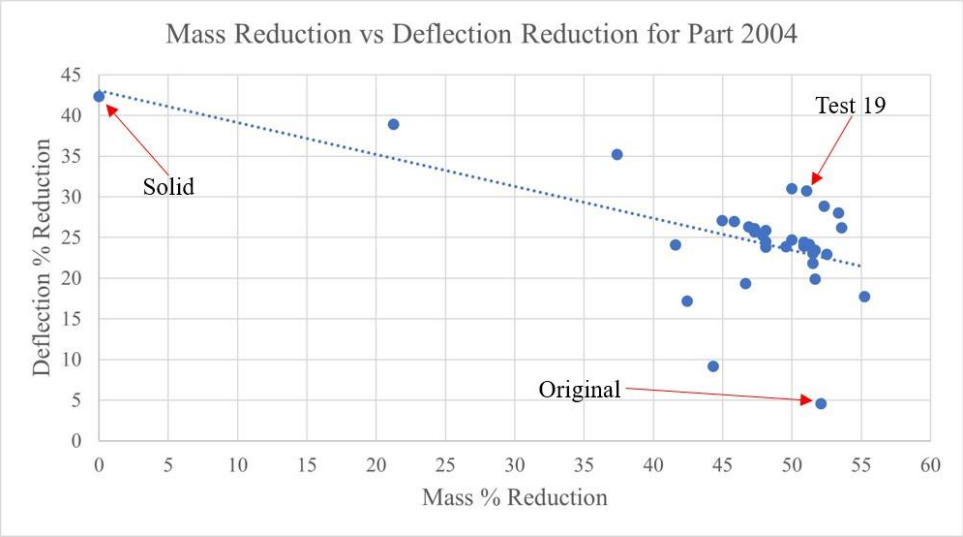

Figure 3-9 Mass and deflection comparison for part 2004. Each point represents the performance of one design. Ideally, there would be a data point in the top right of the graph for max reduction in mass and deflection.

The heaviest version of part 2004 weighed 4.76 kg (completely solid component) while the lightest version weighed 2.13 kg. The total difference in weight between the heaviest and lightest is 2.63 kg. The highest percentage of mass reduction from the heaviest part is 55%. Largest PRISM deflection for the first pose is 0.3766 mm while the smallest amount of deflection is 0.2246 mm with a 0.152 mm difference in deflection. The percentage of deflection reduction from the most deflected link design is 40%. Highest stress occurred near posterior-superior bearing on part 2004. The largest PRISM deflection for the second pose is 0.3400 mm while the smallest amount of deflection is 0.1894 mm with a 0.1506 mm difference in deflection. The percentage of deflection reduction from the most deflected link is 44%. The highest stress location varied between around the two superior bearings on part 2004.

3.3.2 Part 2009 Simulations

The second part analyzed is the input link, 2009. The output and floating links were kept in a constant state for all the trials. The percentage of mass reduction and the percentage of displacement reduction for every design is shown in Figure 3-10. The trend is like the trend seen in Figure 3-9.

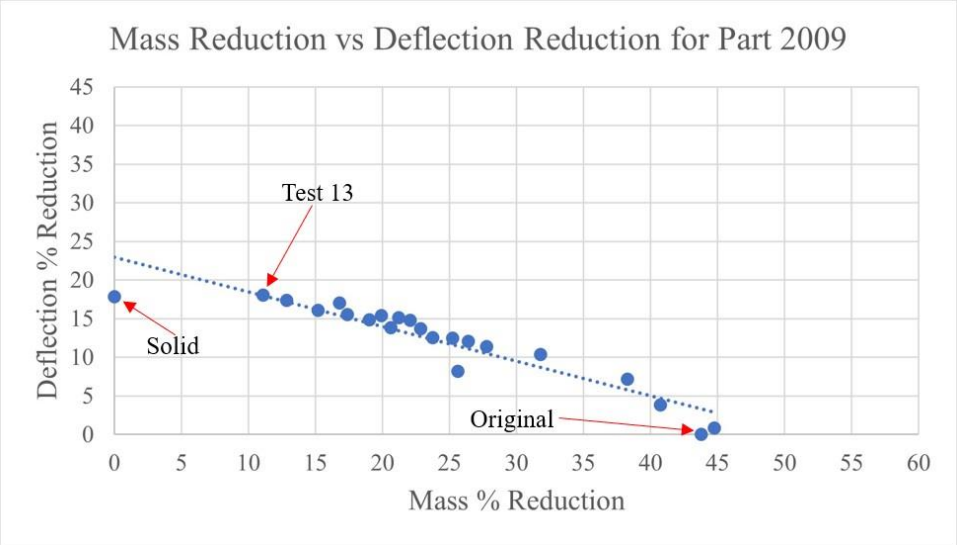

Figure 3-10 Mass and deflection comparison for part 2009. As mass reduction increases, deflection decreases which is an expected behavior.

The heaviest version of part 2009 weighed 1,019 g (completely solid component) while the lightest version weighed 563 g. The total difference in weight between the heaviest and lightest is 456 g. The highest percentage of mass reduction from the heaviest part is 45%. The largest PRISM deflection for the first pose is 0.3321 mm while the smallest amount of deflection is 0.279 mm with a 0.0531 mm difference in deflection. The percentage of deflection reduction from the most deflected design is 16%. The largest PRISM deflection for the second pose is 0.2731 mm while the smallest amount of deflection is 0.2192 mm with a 0.0531 mm difference in deflection. The percentage of deflection reduction from the most deflected design is 18%. The highest stress in both poses is located near the posterior-superior bearing on part 2004.

3.3.3 Part 2010 Simulations

The third part analyzed is the floating link. The input and output links were kept in a constant state for all the trials, but all three floating links were altered. The percentage of mass reduction and the percentage of displacement reduction for every design is illustrated in Figure 3-11. The trend is unlike the trends seen in Figure 3-9 and Figure 3-10. There are designs with high reductions in both deflection and mass.

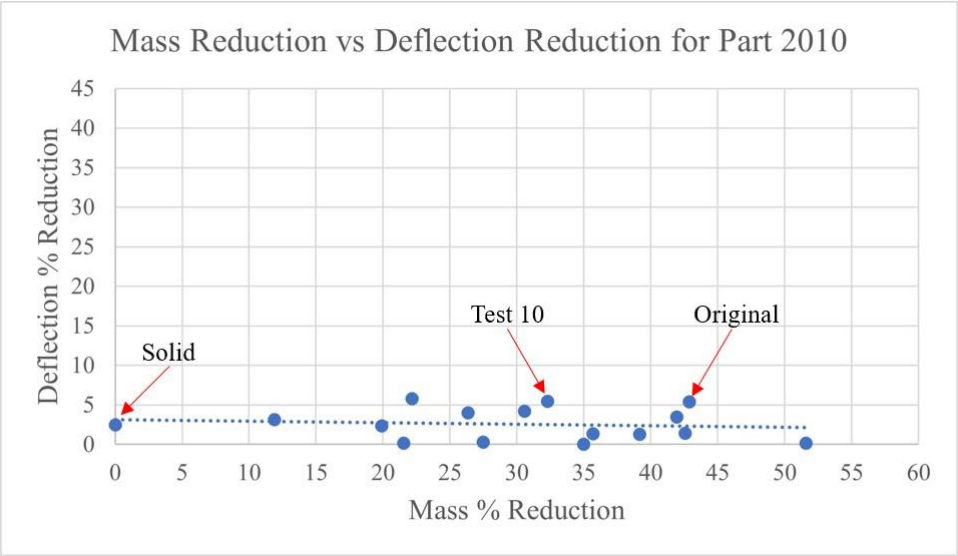

Figure 3-11 Mass and deflection comparison for part 2010. This component has very little effect on the deflection of PRISM. The data also has the least steep downward trend. Several components with less mass outperform components with more mass.

The heaviest version of part 2010 weighed 975 g (completely solid component) while the lightest version weighed 472 g. The total difference in weight between the heaviest and lightest is 503 g. The highest percentage of mass reduction from the heaviest part is 52%. The largest PRISM deflection for the first pose is 0.2851 mm while the smallest amount of deflection is 0.2686 mm with a 0.0165 mm difference in deflection. The percentage of deflection reduction from the most deflected design is 6%. The largest PRISM deflection for the second pose is 0.2245 mm while the smallest amount of deflection is 0.2115 mm with a 0.013 mm difference in deflection. The percentage of deflection reduction from the most deflected design is 6%. The highest stress in both poses is located near the posterior-superior bearing on part 2004.

3.4 Discussion

The main concern for selecting the best design is balancing mass reduction and deflection reduction for each of the three separate parts. There is an expected inverse relationship between mass reduction and deflection reduction. This expected behavior is illustrated by the trendline in Figure 3-9 and Figure 3-10. This relationship is not present for the floating links because these links experience the least stress of the evaluated components and thus have the least influence in deflection change. It is also clear that the output link has the most significant effect on both mass and deflection out of the three evaluated components. The input link, 2009, has a greater effect on deflection than the floating link, but

the floating link can reach three times the mass reduction as the input link because it is implemented three times in each side of PRISM instead of once.

A cost function, like equation (2) presented in chapter 2, is one method to evaluate the various link designs. Important design characteristics for the link components are mass and deflection in two poses. The resulting cost function is:

$$P_i = W_m\left(1-\left(\frac{m_i-m_{min}}{m_{max}-m_{min}}\right)\right)+W_d\left(1-\left(\frac{d_i-d_{min}}{d_{max}-d_{min}}\right)\right)+W_D\left(1-\left(\frac{D_i-D_{min}}{D_{max}-D_{min}}\right)\right) \quad (3)$$

where *P* represents the performance of the link design, *i* represents the ith component, *W* represents the weight of the variable within the cost function, *m* represents the mass of the individual deflection, *d* represents the deflection of PRISM in pose 1, and *D* represents the deflection of PRISM in pose 2. Each design, for all components, is evaluated by three separate weighting distributions. Table 3-2 displays the selecting weighting distributions.

Table 3-2 Cost function analysis for link design. The weights are selected to prioritize deflection over mass. Each characteristic is evaluated based on the best and worst performing link designs in each category.

Link Cost Function Weighting Distributions			
Trial #:	**Mass:**	**Deflection 1:**	**Deflection 2:**
1	0.2	0.4	0.4
2	0.3	0.35	0.35
3	0.4	0.3	0.3

The evaluation of each link component resulted in the selection of the best performing designs for each component: 2004 Test 19, 2009 Test 13, and 2010 Original. These specific designs are the best FEA designs out of the 35, 22, and 16 respective designs for each component. The number of designs for each component correlates with the impact on deflection. As it became clear that deflection was changing less with each component, less models were created for evaluation. Images of all designs can be found in Appendix B, but the selected designs are shown in Figure 3-12.

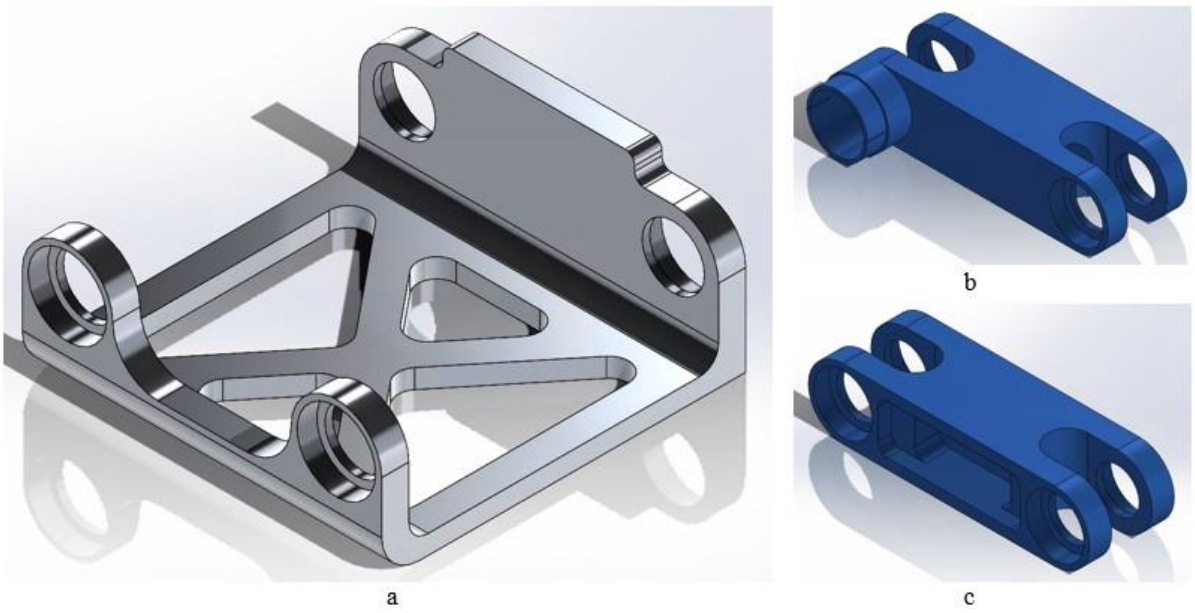

Figure 3-12 Final designs from FEA analysis and cost function evaluation. (a) Part 2004 Test 19. (b) Part 2009 Test 13. (c) Part 2010 Original.

While these designs are the best performing models, there are infinitely more potential designs. The designs were based on keeping key geometry while removing excess material. This process was primarily fueled through intuition. For these simulations, mesh control improved the mesh and accuracy of results, but consistent results could still be gathered from a simulation without mesh control.

3.5 Final Part Design

The goal of the FEA design process was to improve the mass and deflection of the original design. The mass of all FEA components in the final design of PRISM is 14.086 kg. This is a 389 g increase over the original mass of PRISM and less than 3% increase in mass. The average deflection from the two worst-case poses in the final design is 0.2145 mm while the original design has an average deflection of 0.3619 mm. The precent decrease in deflection is 39%. Overall, the deflection was reduced significantly while the mass slightly increased.

Chapter 4: Conclusion

The goal of the research was to design a new gravity assistance system and lower the deflection of PRISM while minimizing change in mass. Designs that accomplish both were presented in Chapters 2 and 3. This chapter will summarize beneficial alterations and future work on this project.

4.1 Collision Prevention Design Alterations

The current base attachment to PRISM creates a collision point with the 1005 sub-assembly and part 2020. One proposed solution is to limit the range of motion of BLUE SABINO. Hardware and software stops would prevent the collision but also limit the motion of the exoskeleton. An alternative solution is to modify the design of BLUE SABINO. There are four potential ways to modify the design to prevent this collision. The first option is to move the entire system further forward on the base attachment. The posterior end of PRISM is already set flush with the base structure so shifting BLUE SABINO forward requires an attachment plate. The second option is to redesign the output link on PRISM, part 2004. A link that extended a few inches forward would allow for the current BLUE SABINO components to attach an anterior part of the output link. The third option is to redesign the attachment part in between PRISM and the rest of BLUE SABINO, part 2020. An extended attachment piece would attach in similar locations to the current design but would require length and design modifications to avoid key features on the output link. The fourth option is to create an alternative tower on the outside of PRISM and shorten the existing base structure. The spring attachment would attach on the exterior of PRISM instead of the interior of PRISM. The second and third options would still require hard stops to prevent the collision with part 2021. Figure 4-1 is a visual of all four potential designs.

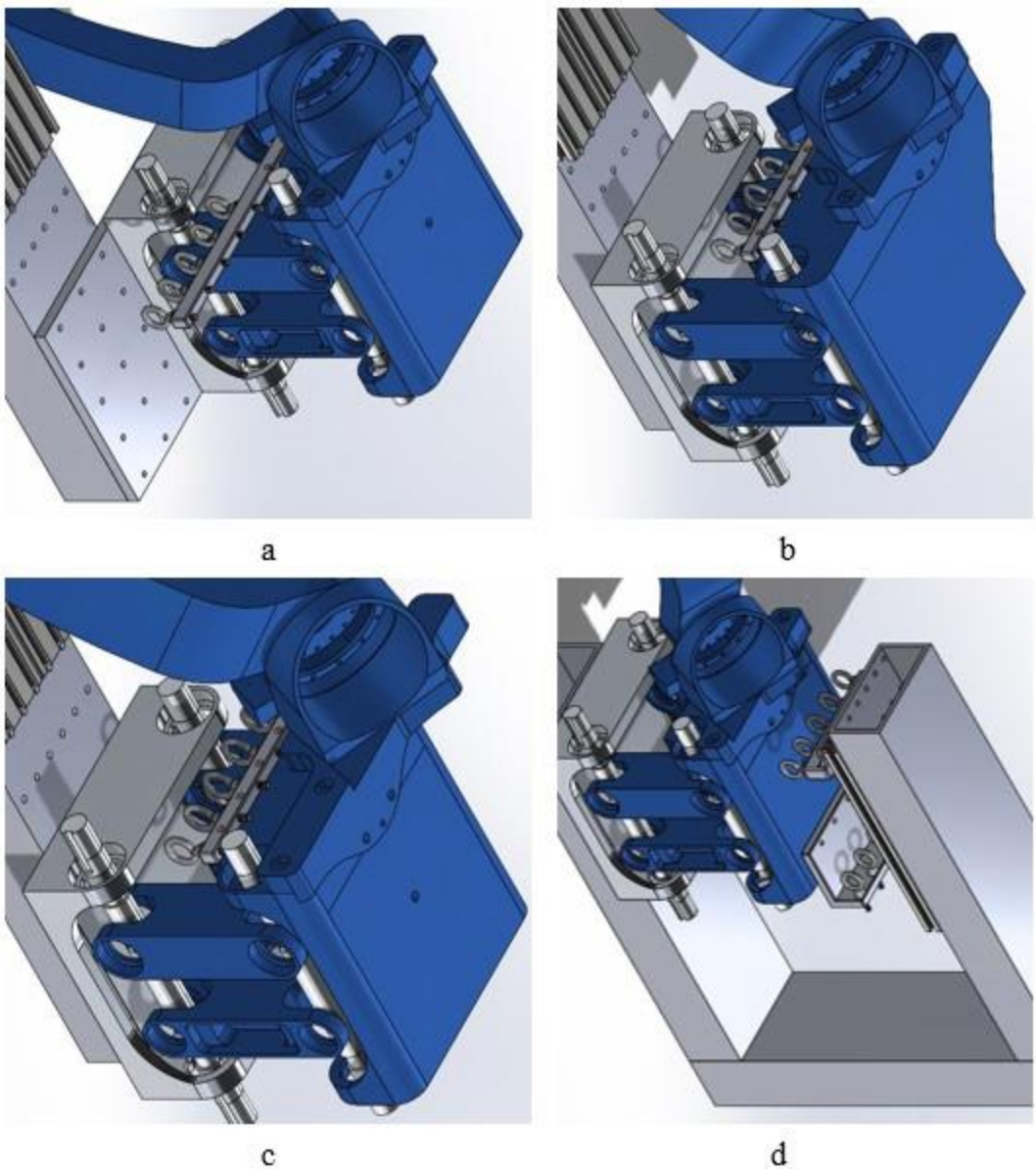

Figure 4-1 Four potential collision solutions. (a) Connection plate. (b) Output link (part 2004) modification. (c) Attachment link (part 2018) modification. (d) Second base tower.

All proposed design modifications have significant implications on the work presented in this thesis. An attachment plate would require altering the spring attachment to keep the springs aligned with the base structure and recalculating the torque implications for Joints 1 and 2 in the new configuration. The analysis performed in chapter 3 is still accurate as the distal joints of BLUE SABINO do not move relative to PRISM. An altered PRISM output link could have the same spring attachment, but it makes the simulation design work obsolete because the loading on PRISM and the design of a key component change. An

altered attachment piece could also have the same spring attachment. FEA on PRISM would be inaccurate as the loading on PRISM from BLUE SABINO is offset from the original analysis. A second tower would require new calculations for torque implications on Joints 1 and 2 from the springs. The FEA results would be accurate, but more design work is required for this tower and spring attachment. I would recommend the second tower.

4.2 Future Work

The goal of PRISM is to activate scapulohumeral rhythm. Currently, PRISM only exists in software. An alteration to prevent the 1005 sub-assembly collision with the attachment tower is the next essential step. There is also still minor design work in PRISM. Almost every part within PRISM has received modifications to account for different sized bearings. These modifications should be checked before manufacturing begins. The holes for attachment to the base (in part 2003) and the rest of BLUE SABINO (in part 2004) have intentionally been excluded. These holes will vary depending on the selected solution to the 1005 sub-assembly collision. The holes in part 2004 for spring attachment will also need to be modified depending on the selected solution to the 1005 sub-assembly collision. The motor connections for both Joints 1 and 2 need to be reevaluated. The motor size for Joint 2 has increased, but not all surrounding parts have been altered to accommodate the change. The primary support component could also be redesigned as it currently requires a lot of material and provides questionable amounts of support. There is currently no design for hard stops on either joint of PRISM which is a key safety feature for the operator of BLUE SABINO. The entire design of PRISM has only been evaluated through software. Upon manufacturing, the entire spring design should be evaluated, starting with the spring force estimates for control. The 8020 components within the spring attachment should be replaced once validated for a better connection.

4.3 Concluding Remarks

In summary, this thesis proposes a thorough design for Joint 2 gravity compensation and for PRISM links. The proposed gravity compensation solution reduces torque requirements, maintains actuator placement, considers ergonomics, and improves safety. Replacing ball bearings with tapered-roller bearings increases the rigidity of PRISM. FEA of new PRISM links estimates a decrease in deflection by 39% from the original design. This

design still needs modification to prevent collisions, but it presents a simple solution to gravity balancing Joint 2 in PRISM and decreasing deflection at the end-effector.

References

American Heart Association. (2019, May 14). *Rehab Therapy After a Stroke*. American Stroke Association. https://www.stroke.org/en/life-after-stroke/stroke-rehab/rehab-therapy-after-a-stroke

Ball, S. J., Brown, I. E., & Scott, S. H. (2007). MEDARM: A rehabilitation robot with 5DOF at the shoulder complex. *IEEE/ASME International Conference on Advanced Intelligent Mechatronics, AIM*, 1–6. https://doi.org/10.1109/AIM.2007.4412446

Bitikofer, C. (2018). *Mapping ADL Motion Capture Data to BLUE SABINO Exoskeleton Kinematics and Dynamics* [Thesis]. University of Idaho.

Bitikofer, C. K., Wolbrecht, E. T., & Perry, J. C. (2018). Mapping ADL Motion Capture Data to BLUE SABINO Exoskeleton Kinematics and Dynamics. *Proceedings of the Annual International Conference of the IEEE Engineering in Medicine and Biology Society, EMBS, 2018-July*, 4914–4919. https://doi.org/10.1109/EMBC.2018.8513164

Branz, A. J. (2019). *Finite Element Analysis Validation in Ball Bearing and Linkage Assemblies for Exoskeleton Robotics* [Thesis]. University of Idaho.

Carignan, C., Tang, J., Roderick, S., & Naylor, M. (2007). A Configuration-Space Approach to Controlling a Rehabilitation Arm Exoskeleton. *2007 IEEE 10th International Conference on Rehabilitation Robotics*, 179–187.

Colombo, R., & Sanguineti, V. (Eds.). (2018). Rehabilitation Robotics: Technology and Applications. In *Rehabilitation Robotics: Technology and Applications* (pp. xix–xxvi). Academic Press. https://doi.org/10.1016/B978-0-12-811995-2.09991-4

GBD 2016 Stroke Collaborators. (2019). Global, regional, and national burden of stroke, 1990-2016. *Lancet*, *18*, 439–458.

Hall, M. J., Levant, S., & Defrances, C. J. (2012). *Hospitalization for Stroke in U.S. Hospitals, 1989-2009*.

Herder, J. L. (2001). *Energy-free Systems; Theory, conception and design of statically balanced spring mechanisms*. https://doi.org/10.13140/RG.2.1.3942.8966

Hill, P. W. (2019). *Gravity Compensation of an Exoskeleton Joint Using Constant-Force Springs* [Thesis]. University of Idaho.

Hill, P. W., Bitikofer, C. K., Trimble, S. T., Wolbrecht, E. T., & Perry, J. C. (2019). Pandora: Design of a 2-dof scapulohumeral exoskeleton device to support translation of the glenohumeral joint. In L. Masia, S. Micera, M. Akay, & J. L. Pons (Eds.), *Biosystems and Biorobotics* (ICNR 2018, Vol. 21, pp. 488–492). Springer, Cham. https://doi.org/10.1007/978-3-030-01845-0_98

Jackson, G., & Chari, K. (2019). *National Hospital Care Survey Demonstration Projects: Stroke Inpatient Hospitalizations*. https://www.cdc.gov/nchs/products/index.htm.

Kim, B., & Deshpande, A. D. (2017). An upper-body rehabilitation exoskeleton Harmony with an anatomical shoulder mechanism: Design, modeling, control, and performance evaluation. *International Journal of Robotics Research*, *36*(4), 414–435. https://doi.org/10.1177/0278364917706743

Krebs, H. I., & Volpe, B. T. (2013). Rehabilitation Robotics. In M. P. Barnes & D. C. Good (Eds.), *Handbook of Clinical Neurology* (Vol. 110, pp. 283–294). Elsevier. https://doi.org/10.1016/B978-0-444-52901-5.00023-X

Lackland, D. T., Roccella, E. J., Deutsch, A. F., Fornage, M., George, M. G., Howard, G., Kissela, B. M., Kittner, S. J., Lichtman, J. H., Lisabeth, L. D., Schwamm, L. H., Smith, E. E., & Towfighi, A. (2014). Factors influencing the decline in stroke mortality a statement from the american heart association/american stroke association. *Stroke*, *45*(1), 315–353. https://doi.org/10.1161/01.str.0000437068.30550.cf

Langhorne, P., Bernhardt, J., & Kwakkel, G. (2011). Stroke Care 2: Stroke rehabilitation. In *Lancet* (Vol. 377). http://www.ebrsr.com

Maciejasz, P., Eschweiler, J., Gerlach-Hahn, K., Jansen-Troy, A., & Leonhardt, S. (2014). A survey on robotic devices for upper limb rehabilitation. *Journal of NeuroEngineering and Rehabilitation*, *11*(3). http://www.jneuroengrehab.com/content/11/1/3

Meshing Options - 2023 - SOLIDWORKS Help. (2023). SOLIDWORKS Help. https://help.solidworks.com/2023/english/SolidWorks/cworks/c_Meshing_Options.htm?verRedirect=1

Murphy, S. L., Kochanek, K. D., Xu, J., & Arias, E. (2020). *Mortality in the United States, 2020 Key findings Data from the National Vital Statistics System*. https://www.cdc.gov/nchs/products/index.htm.

Murray, R. M., Li, Z., & Sastry, Shankar. (1994). *A mathematical introduction to robotic manipulation*. CRC Press.

National Aeronautics and Space Administration. (1995). Anthropometry and Biomechanics. In *Man-systems Integration Standards: Vol. I* (B).

Park, H.-S., Ren, Y. R., & Zhang, L.-Q. (2008). IntelliArm: An Exoskeleton for Diagnosis and Treatment of Patients with Neurological Impairments. *2008 2nd IEEE RAS & EMBS International Conference on Biomedical Robotics and Biomechatronics*, 109–114.

Perry, J. C., Maura, R., Bitikofer, C. K., & Wolbrecht, E. T. (2019). Blue sabino: Development of a bilateral exoskeleton instrument for comprehensive upper-extremity neuromuscular assessment. In L. Masia, S. Micera, M. Akay, & J. L. Pons (Eds.), *Biosystems and Biorobotics* (ICNR 2018, Vol. 21, pp. 493–497). Springer, Cham. https://doi.org/10.1007/978-3-030-01845-0_99

Perry, J. C., Rosen, J., & Burns, S. (2007). Upper-limb powered exoskeleton design. *IEEE/ASME Transactions on Mechatronics*, *12*(4), 408–417. https://doi.org/10.1109/TMECH.2007.901934

Petrock, S. (2020, July 2). *SOLIDWORKS Simulation Makes Meshing Easy. Too Easy?* Technology for Design and Engineering.

Sanchez, R. J., Wolbrecht, E., Smith, R., Liu, J., Rao, S., Cramer, S., Rahman, T., Bobrow, J. E., Reinkensmeyer, D. J., & Shah, P. (2005). A pneumatic robot for re-training arm movement after stroke: Rationale and mechanical design. *Proceedings of the 2005 IEEE*

9th International Conference on Rehabilitation Robotics, 2005, 500–504. https://doi.org/10.1109/ICORR.2005.1501151

Schaeffler Group USA. (n.d.). *Rigidity | Schaeffler medias*. Retrieved November 5, 2022, from https://medias.schaeffler.us/en/rigidity

Schiele, A., & van der Helm, F. C. T. (2006). Kinematic design to improve ergonomics in human machine interaction. *IEEE Transactions on Neural Systems and Rehabilitation Engineering*, *14*(4), 456–469. https://doi.org/10.1109/TNSRE.2006.881565

Shen, Y., Ma, J., Dobkin, B., & Rosen, J. (2018). Asymmetric Dual Arm Approach for Post Stroke Recovery of Motor Functions Utilizing the EXO-UL8 Exoskeleton System: A Pilot Study. *2018 40th Annual International Conference of the IEEE Engineering in Medicine and Biology Society (EMBC)*, 1701–1707. https://doi.org/10.0/Linux-x86_64

Trimble, S. T. (2016). *PANDORA: Design of a 2 DOF Scapulohumeral Device* [Thesis]. Univeristy of Idaho.

Tsao, C. W., Aday, A. W., Almarzooq, Z. I., Alonso, A., Beaton, A. Z., Bittencourt, M. S., Boehme, A. K., Buxton, A. E., Carson, A. P., Commodore-Mensah, Y., Elkind, M. S. V., Evenson, K. R., Eze-Nliam, C., Ferguson, J. F., Generoso, G., Ho, J. E., Kalani, R., Khan, S. S., Kissela, B. M., … Martin, S. S. (2022). Heart Disease and Stroke Statistics—2022 Update: A Report From the American Heart Association. *Circulation*, *145*(8). https://doi.org/10.1161/CIR.0000000000001052

Vespa, J. (2018, March 13). *The U.S. Joins Other Countries With Large Aging Populations*. https://www.census.gov/library/stories/2018/03/graying-america.html

Wolbrecht, E. T., Leavitt, J., Reinkensmeyer, D. J., & Bobrow, J. E. (2006). Control of a Pneumatic Orthosis for Upper Extremity Stroke Rehabilitation. *Annual International Conference of the IEEE Engineering in Medicine and Biology - Proceedings*, 2687–2693. https://doi.org/10.1109/IEMBS.2006.259941

Zeiler, S. R. (2019). Should We Care About Early Post-Stroke Rehabilitation? Not Yet, but Soon. In *Current Neurology and Neuroscience Reports* (Vol. 19, Issue 3). Current Medicine Group LLC 1. https://doi.org/10.1007/s11910-019-0927-x

Appendix A: Torque Calculation

The kinematics of the PRISM mechanism has four rotation axes, but the constraints of the dual-parallel mechanisms reduce the motion to 2-DOF. Presented kinematics are for the right arm of BLUE SABINO. The spatial frame and output frame are defined in Figure A-1.

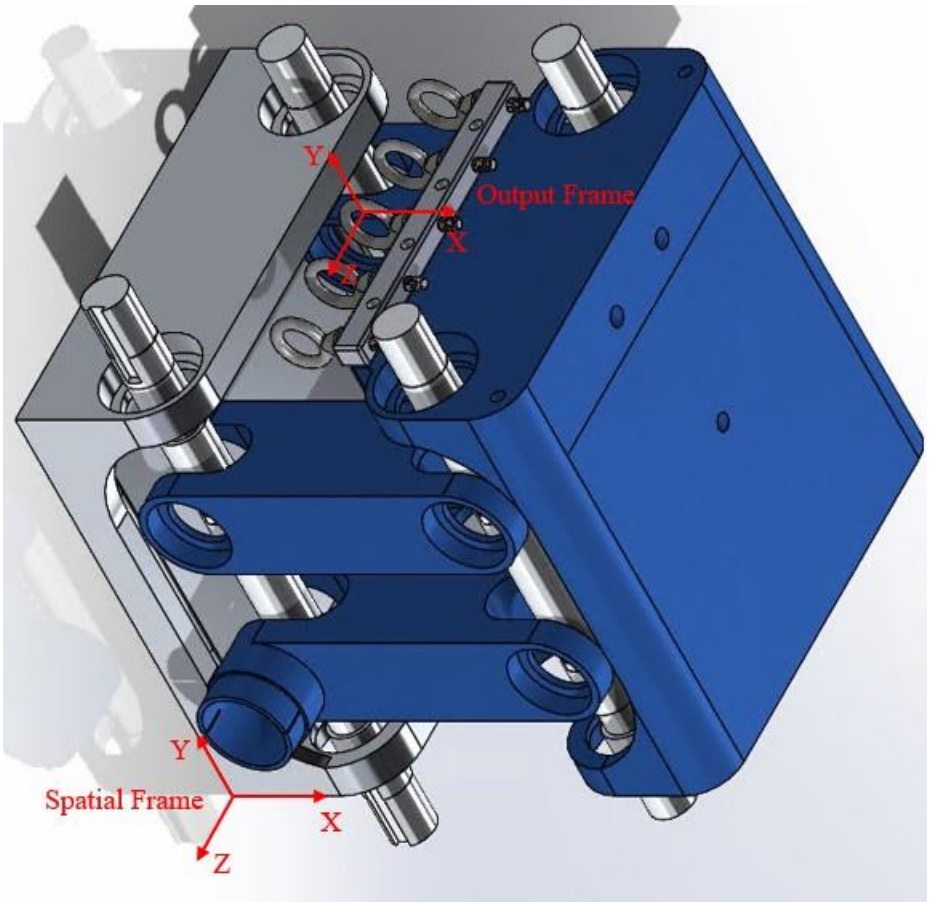

Figure A-1 The spatial frame is attached to part 2003 and the output frame is attached to the central spring connection eyebolt. The axes extend in the same directions for both coordinate frames.

The output frame is fixed at the top of the eyebolt. This provides an approximation for the spring length, spring force direction, and spring force location because the spring is aligned with the center of the eyebolt (for vertical displacements, not horizontal displacements) instead of the top of the eyebolt. The maximum error for spring length, spring force direction, and spring force location are 0.2-mm, 0.46-deg, and 1.36-mm, respectively. All three of these maximum errors occur at 0-deg protraction/retraction and 15-deg elevation. The maximum percent error in the spring length is 0.06%. Tracking the motion of the output frame is

achieved through tracking the distal connection point between part 2009 and part 2008 because of the dual-parallel mechanism. In the home position, the rotation axes (defined relative to the spatial frame) of the dual-parallel mechanism are:

$$w_1 = \begin{bmatrix}0\\1\\0\end{bmatrix}, w_2 = \begin{bmatrix}0\\0\\-1\end{bmatrix}, w_{2b} = \begin{bmatrix}0\\0\\1\end{bmatrix}, w_{1b} = \begin{bmatrix}0\\-1\\0\end{bmatrix}. \quad (4)$$

The actuated axes are w_1 and w_2 and the rotation angle about each axis are defined as θ_1 and θ_2, respectively. The location of these axes relative to the spatial frame are:

$$q_1 = \begin{bmatrix}60\\0\\-30\end{bmatrix}, q_2 = \begin{bmatrix}60\\73.5\\0\end{bmatrix}, q_{2b} = \begin{bmatrix}212.4\\73.5\\0\end{bmatrix}, q_{1b} = \begin{bmatrix}212.4\\0\\-30\end{bmatrix} (mm). \quad (5)$$

The rigid body transformation to the home position of the output frame is established at the top inner surface of the eyebolt (the central eyebolt, specifically) for spring connection:

$$g_{ab}(0) = \begin{bmatrix}1 & 0 & 0 & 140.4125\ (mm)\\0 & 1 & 0 & 256.875\ (mm)\\0 & 0 & 1 & -119\ (mm)\\0 & 0 & 0 & 1\end{bmatrix}. \quad (6)$$

Following (Murray et al., 1994), the location and orientation of the output frame is calculated via the product-of-exponentials formulation:

$$g_{ab}(\theta) = e^{\hat{\xi}_1\theta_1}e^{\hat{\xi}_2\theta_2}e^{\hat{\xi}_3\theta_3}e^{\hat{\xi}_4\theta_4}g_{ab}(0) \quad (7)$$

and

$$\bar{r}_a(\theta) = g_{ab}(\theta)\bar{r}_b, \quad (8)$$

where ξ_i is the 6x1 twist ($\xi_i = [-w_i \times q_i \;\; w_i]^T$), $\bar{r}_a(\theta)$ is the 4x1 coordinates of point *r* in the spatial frame, and $\bar{r}_b$ is the 4x1 coordinates of point *r* in the output frame. Point *r* is located at the origin of the output frame. Because of the constraints of a dual-parallel mechanism, the motion of the axes results in $\theta_1 = \theta_{1b}$ and $\theta_2 = \theta_{2b}$. Using these substitutions, $g_{ab}(\theta)$ can be defined as a function of only θ_1 and θ_2.

$$g_{ab}(\theta) = \begin{bmatrix} 1 & 0 & 0 & 152.4\cos\theta_1\cos\theta_2 - 11.9875\ (mm) \\ 0 & 1 & 0 & 256.875 - 152.4\sin\theta_2\ \ (mm) \\ 0 & 0 & 1 & -152.4\cos\theta_2\sin\theta_1 - 119\ (mm) \\ 0 & 0 & 0 & 1 \end{bmatrix} \tag{9}$$

The relationship between joint torques and forces and torques acting on the output frame is derived through virtual work. If friction is neglected, work is the same at the joints and end-effector (Murray et al., 1994):

$$\int_{t_1}^{t_2} \dot{\theta} \cdot \tau \, dt = \ W = \ \int_{t_1}^{t_2} V_{st}^b \cdot F_t \, dt, \tag{10}$$

where W is work, t is time, $V_{st}^b \in \mathrm{R}^6$ is the body velocity of the end-effector, and $F_t \in \mathrm{R}^6$ is the body wrench from the spring force, $\dot{\theta}$ are angular velocities $[\dot{\theta}_1, \dot{\theta}_2, \dot{\theta}_{2b}, \dot{\theta}_{1b}]^T$ and τ are joint torques $[\tau_1, \tau_2, \tau_{2b}, \tau_{1b}]^T$. Considering the integrand is true for all time intervals and $V_{st}^b = J_{st}^b \dot{\theta}$ (where J_{st}^b is the 6x4 spatial Jacobian):

$$\dot{\theta}^T \tau = \ \dot{\theta}^T (J_{st}^b)^T F_t. \tag{11}$$

The resultant joint torque is a 4x1 vector, signifying four actuators instead of two. The joint torque thus needs to be reduced to the two actuated joints. Because $\dot{\theta}_1 = \ \dot{\theta}_{1b}$ and $\dot{\theta}_2 = \ \dot{\theta}_{2b}$, $\dot{\theta}$ can be redefined with reduced angular velocities $\dot{\theta}_r$ (Sanchez et al., 2005):

$$\dot{\theta} \ = \ P\dot{\theta}_r, \tag{12}$$

where:

$$P_{actuator} = \begin{bmatrix} 1 & 0 \\ 0 & 1 \\ 0 & 0 \\ 0 & 0 \end{bmatrix}, P_{spring} = \begin{bmatrix} 1 & 0 \\ 0 & 1 \\ 0 & 1 \\ 1 & 0 \end{bmatrix}, \dot{\theta}_r = \begin{bmatrix} \dot{\theta}_1 \\ \dot{\theta}_2 \end{bmatrix}. \tag{13}$$

Combining equations (11) and (12) results in:

$$(P_{actuator}\dot{\theta}_r)^T \tau = \ (P_{spring}\dot{\theta}_r)^T (J_{st}^b)^T F_t. \tag{14}$$

This equation is simplified into:

$$\dot{\theta}_r{}^T P_{actuator}^T \tau = \ \dot{\theta}_r{}^T P_{spring}^T (J_{st}^b)^T F_t. \tag{15}$$

Because $\dot{\theta}_r$ is free, the resultant relationship between actuator torque and spring force is:

$$P_{actuator}^{T}\tau = P_{spring}^{T}(J_{st}^{b})^{T}F_{t}. \quad (16)$$

The matrix multiplication of $P_{actuator}^{T}$ (2x4) and τ (4x1) reduces the torque to a 2x1 vector representing the two actuated torques.

Appendix B: Part Designs

Part 2004 Designs:

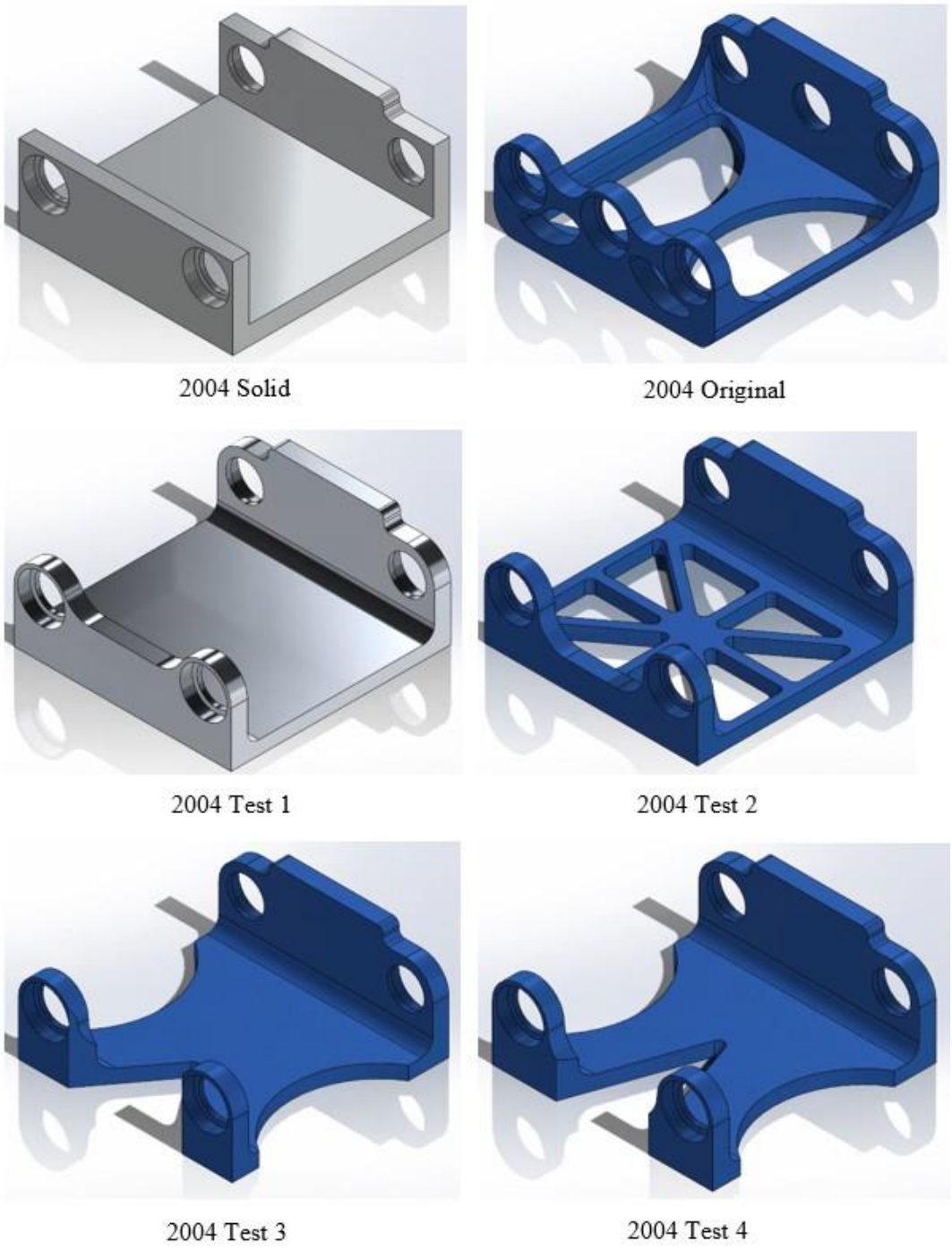

Figure B-1 Part 2004 images 1.

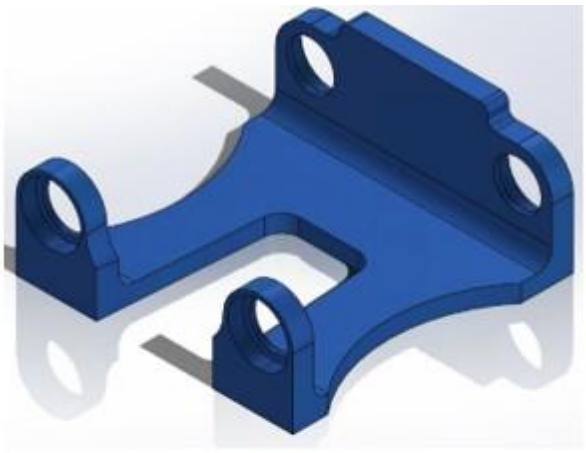

2004 Test 5

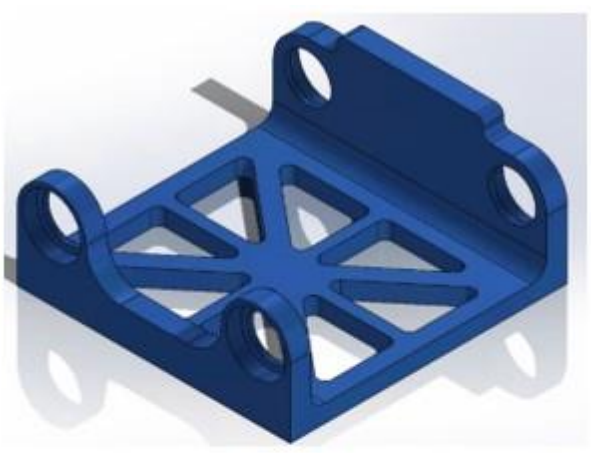

2004 Test 6

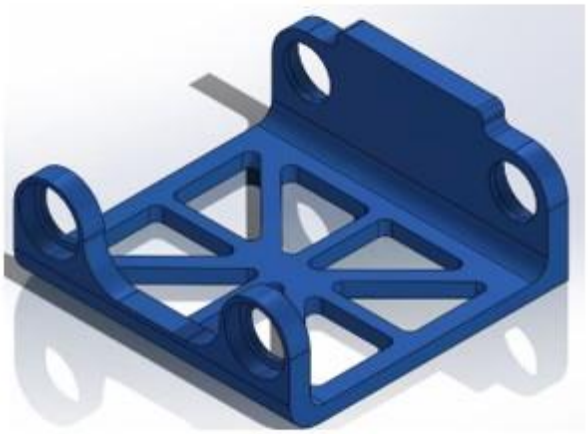

2004 Test 7

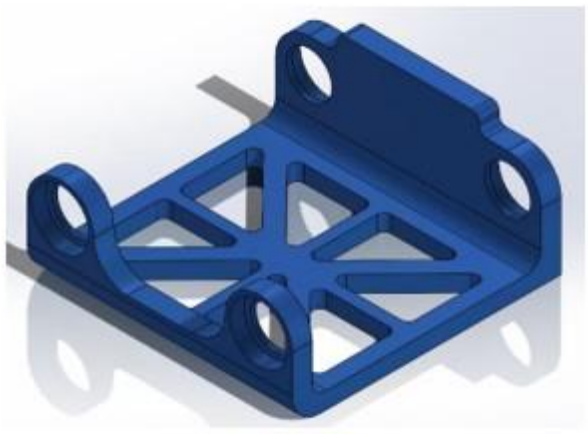

2004 Test 8

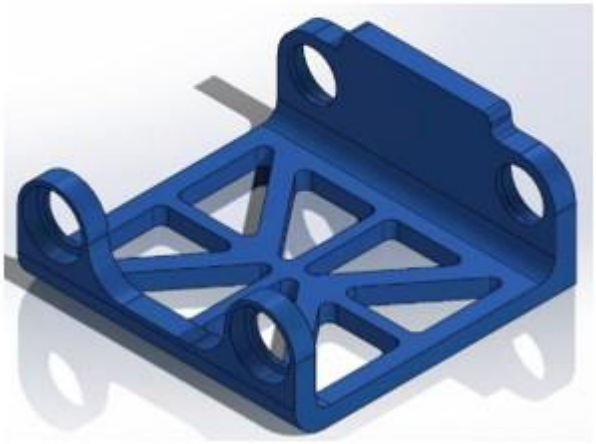

2004 Test 9

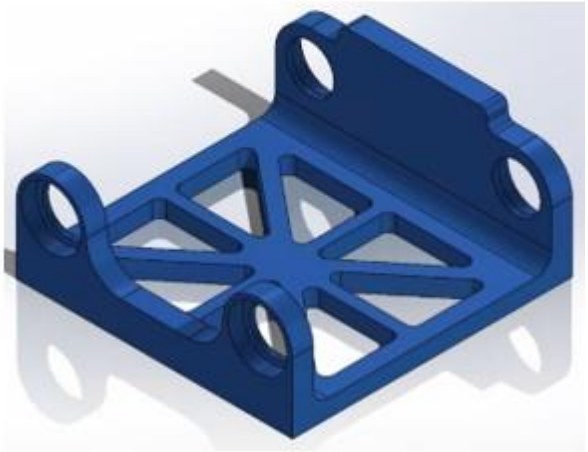

2004 Test 10

Figure B-2 Part 2004 images 2.

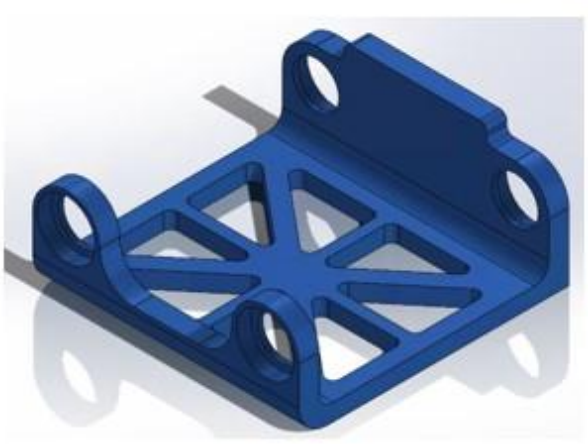

2004 Test 11

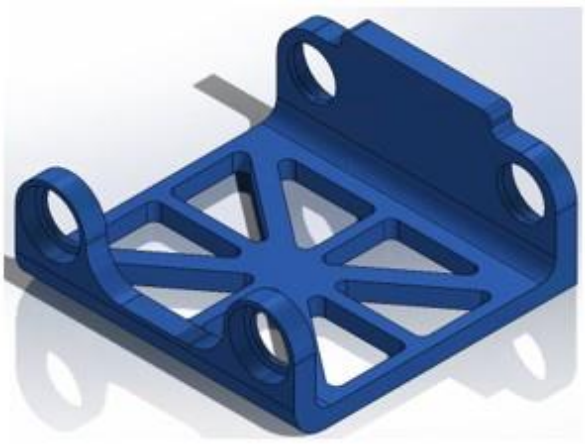

2004 Test 12

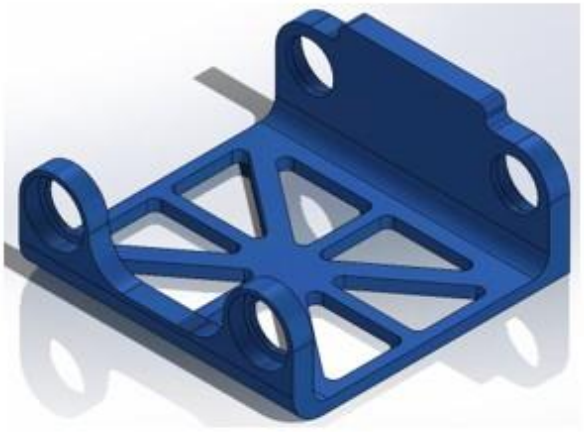

2004 Test 13

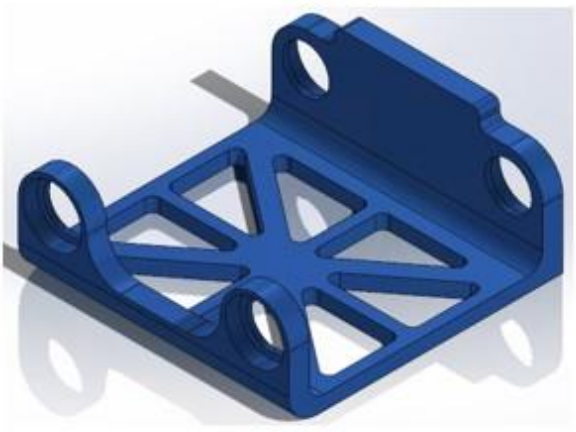

2004 Test 14

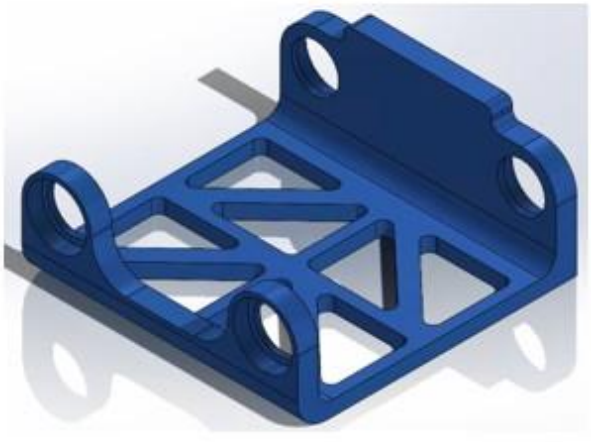

2004 Test 15

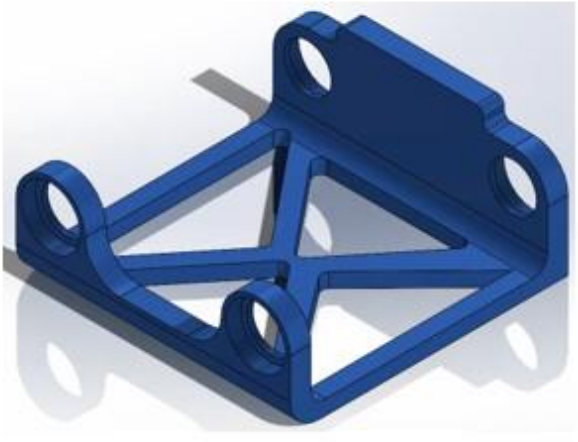

2004 Test 16

Figure B-3 Part 2004 images 3.

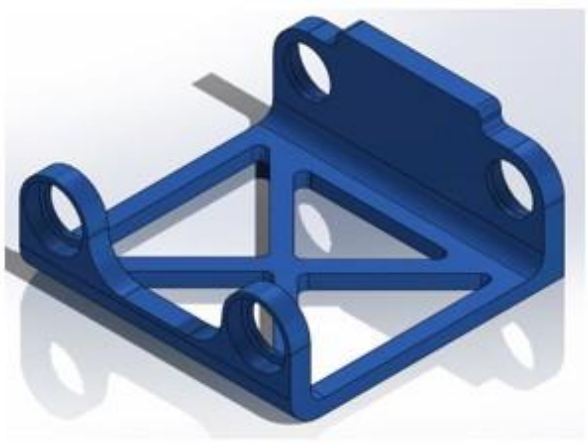

2004 Test 17

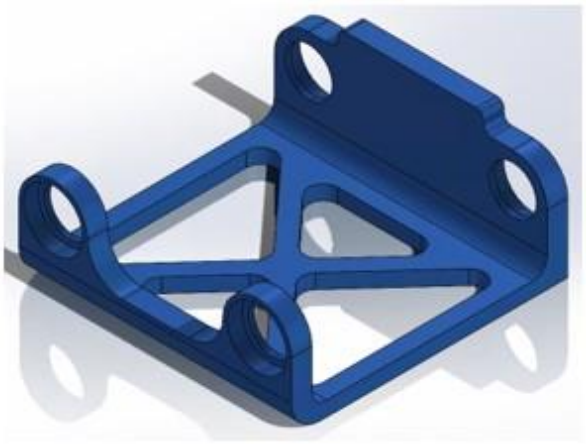

2004 Test 18

2004 Test 19

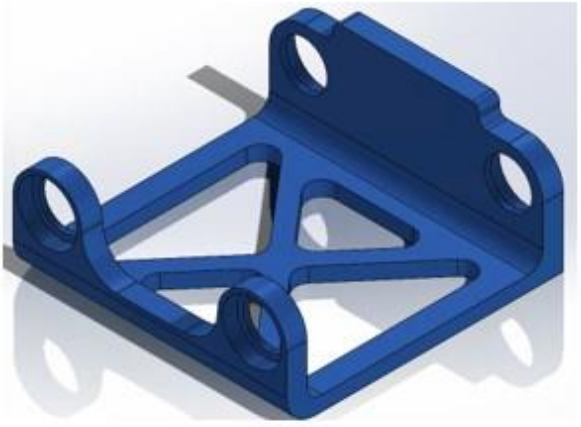

2004 Test 20

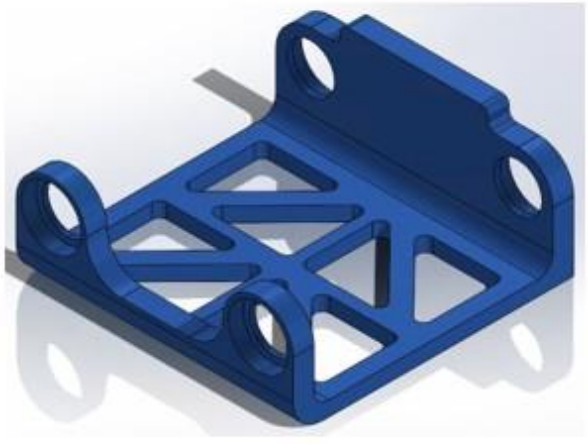

2004 Test 21

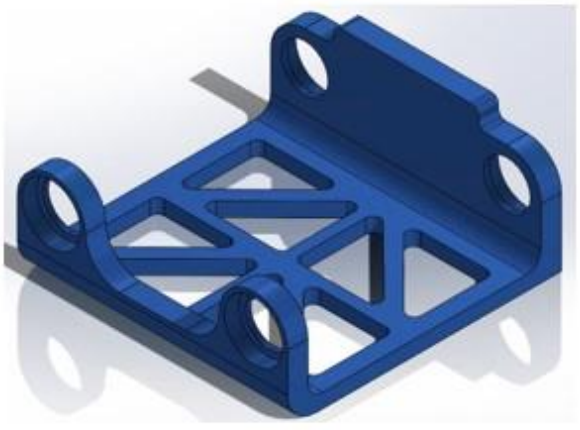

2004 Test 22

Figure B-4 Part 2004 images 4.

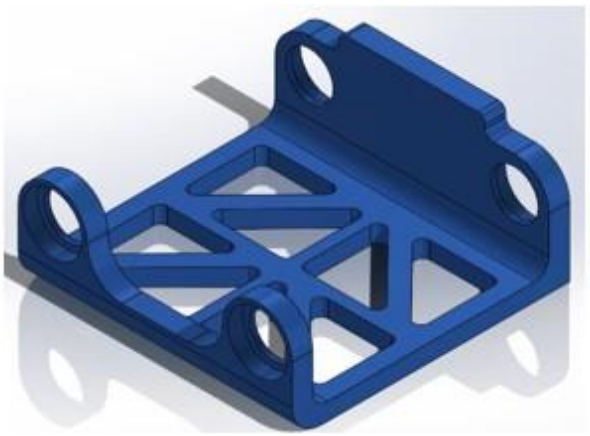

2004 Test 23

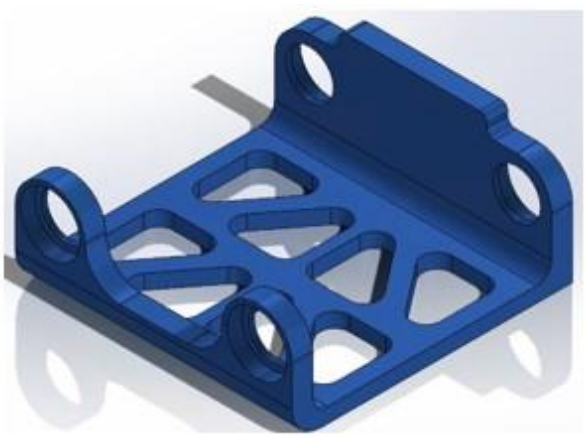

2004 Test 24

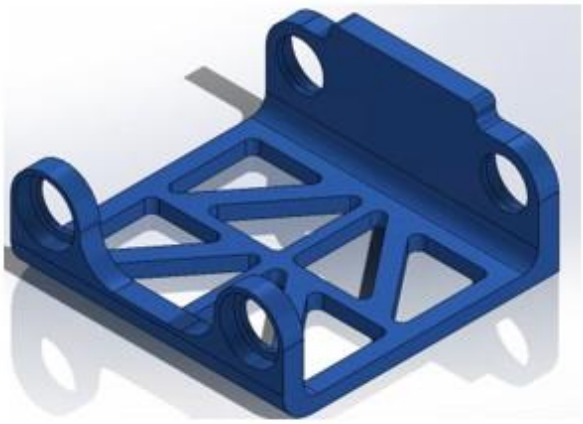

2004 Test 25

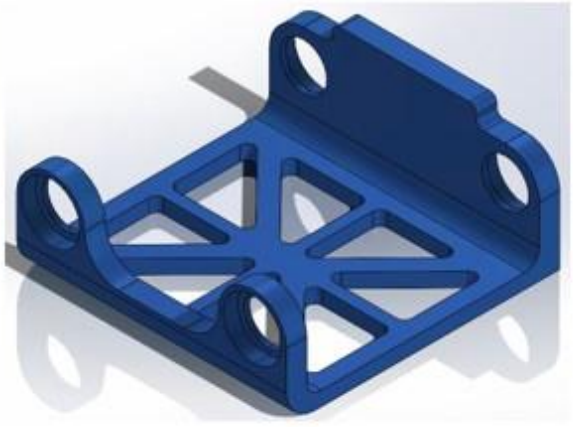

2004 Test 26

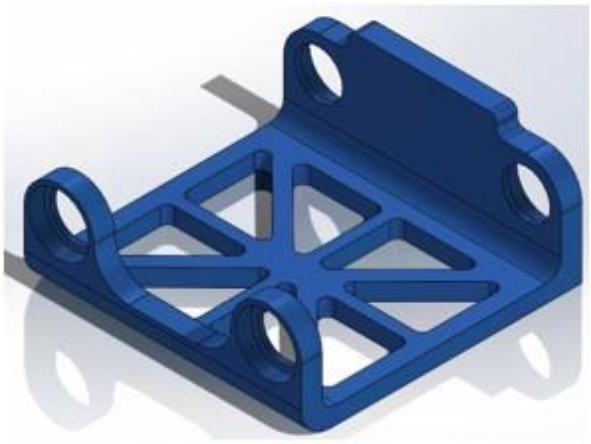

2004 Test 27

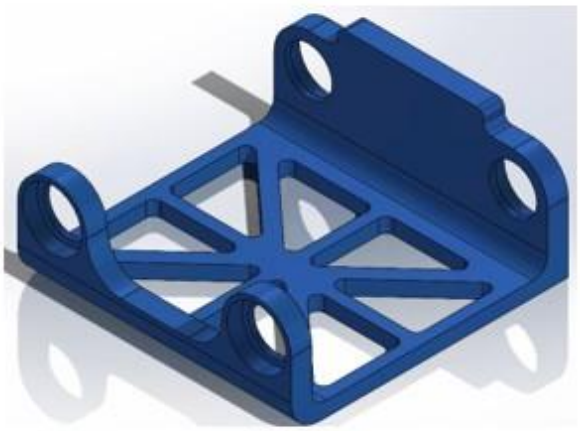

2004 Test 28

Figure B-5 Part 2004 images 5.

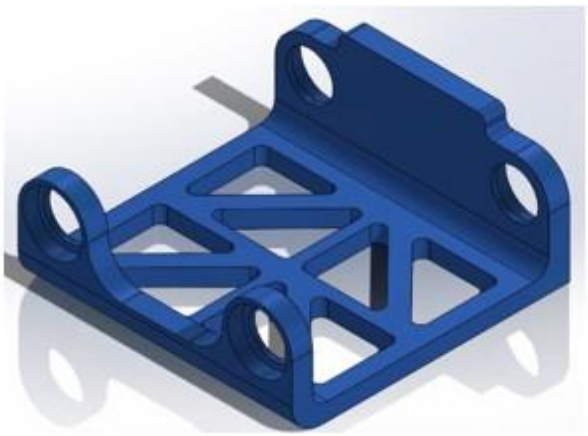

2004 Test 29

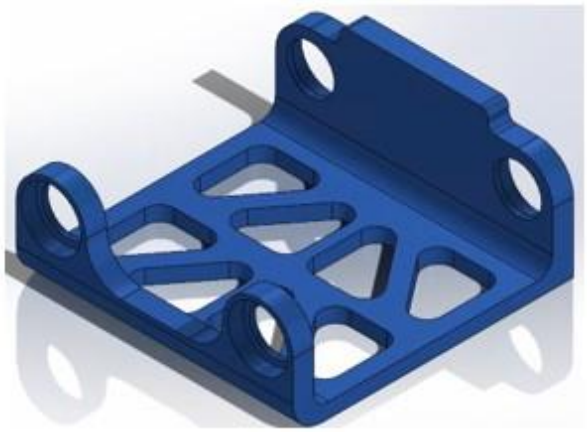

2004 Test 30

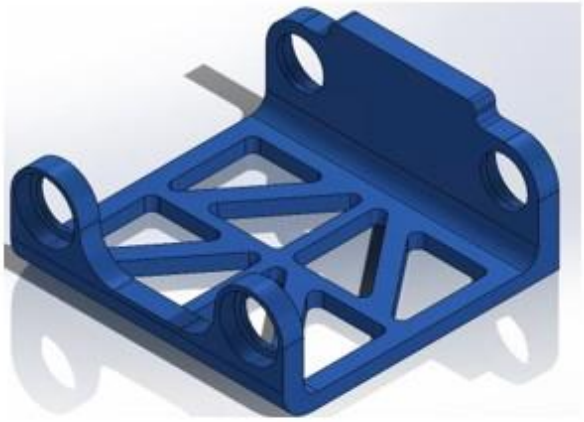

2004 Test 31

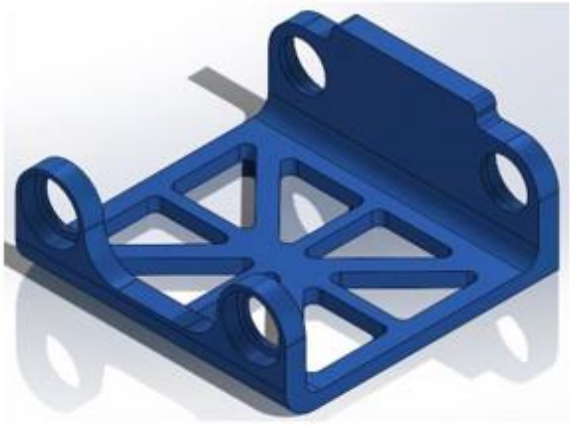

2004 Test 32

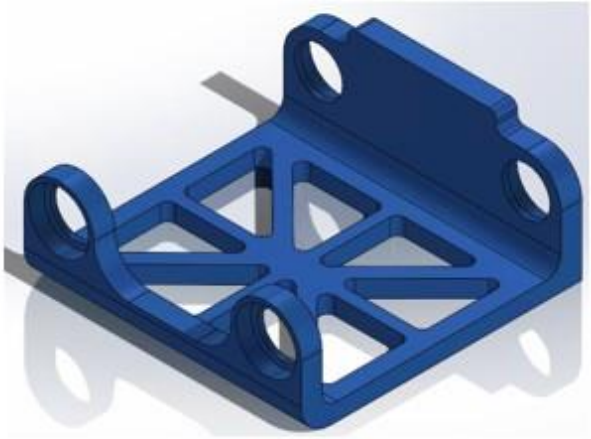

2004 Test 33

Figure B-6 Part 2004 images 6.

Table B-1 Summary of design alterations for part 2004. [1]Designs called pants are visually different from each other and modified parameters do not correlate with other designs. [2]Design labeled X-error is a result of an unnoticed rebuilding error.

Part 2004 Alterations							
Design #:	**Shape:**	**Segment Angle:**	**Thickness:**	**Diagonal Width:**	**Outside Width:**	**Inner Fillets:**	**Outer Fillets:**
1	Solid	N/A	15-mm	N/A	N/A	N/A	None
2	Spider	30	15-mm	10-mm	10-mm	1/4”	None
3	Pants[1]	N/A	15-mm	N/A	N/A	1/4”	None
4	Pants[1]	N/A	15-mm	N/A	N/A	1/4”	None
5	Pants[1]	N/A	15-mm	N/A	N/A	5/8”	None
6	Spider	30	15-mm	15-mm	15-mm	1/4”	None
7	Spider	15	12.7-mm	12.5-mm	15-mm	1/4”	1”
8	Spider	15	15-mm	15-mm	15-mm	1/4”	1”
9	Spider	0	15-mm	15-mm	15-mm	1/4”	1”
10	Spider	30	15-mm	12.5-mm	15-mm	1/4”	None
11	Spider	30	15-mm	15-mm	15-mm	1/4”	1”
12	Spider	30	15-mm	15-mm	10-mm	1/4”	1”
13	Spider	30	10-mm	15-mm	10-mm	1/4”	1”
14	Spider	30	12.7-mm	15-mm	10-mm	1/4”	1”
15	Tree	15	12.7-mm	15-mm	10-mm	1/4”	1”
16	X-Error[2]	15	12.7-mm	Variable	15-mm	1/4”	1”
17	X	0	12.7-mm	15-mm	15-mm	1/4”	1”
18	X	0	12.7-mm	15-mm	15-mm	1/2”	1”
19	X	0	12.7-mm	20-mm	20-mm	1/2”	1”
20	X	0	12.7-mm	15-mm	20-mm	1/2”	1”
21	Tree	15	12.7-mm	15-mm	15-mm	1/4”	1”
22	Tree	15	12.7-mm	12.5-mm	15-mm	1/4”	1”
23	Tree	15	15-mm	15-mm	15-mm	1/4”	1”
24	Tree	15	12.7-mm	15-mm	15-mm	1/2”	1”
25	Tree	0	12.7-mm	15-mm	15-mm	1/4”	1”
26	Spider	15	12.7-mm	15-mm	15-mm	1/4”	1”
27	Spider	15	15-mm	12.5-mm	15-mm	1/4”	1”
28	Spider	15	12.7-mm	12.5-mm	10-mm	1/4”	1”
29	Spider	15	12.7-mm	12.5-mm	15-mm	1/4”	1/2”
30	U-Tree	15	12.7-mm	12.5-mm	15-mm	1/4”	1”
31	X	0	12.7-mm	20-mm	25-mm	1/2”	1”
32	Solid	N/A	9.525-mm	N/A	N/A	N/A	1/2”
33	Solid	N/A	6.35-mm	N/A	N/A	N/A	1/2”

Part 2009 Designs:

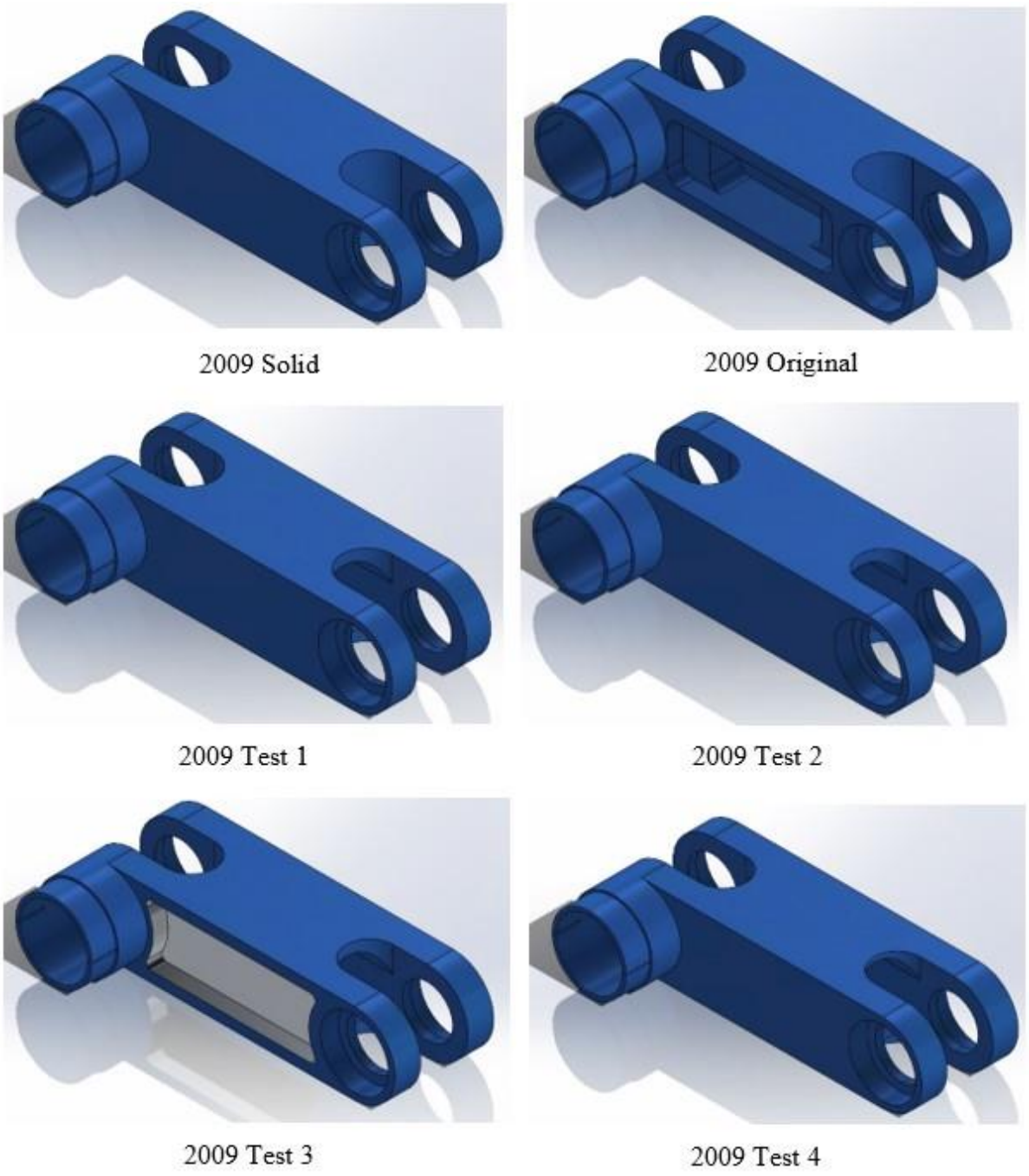

Figure B-7 Part 2009 images 1.

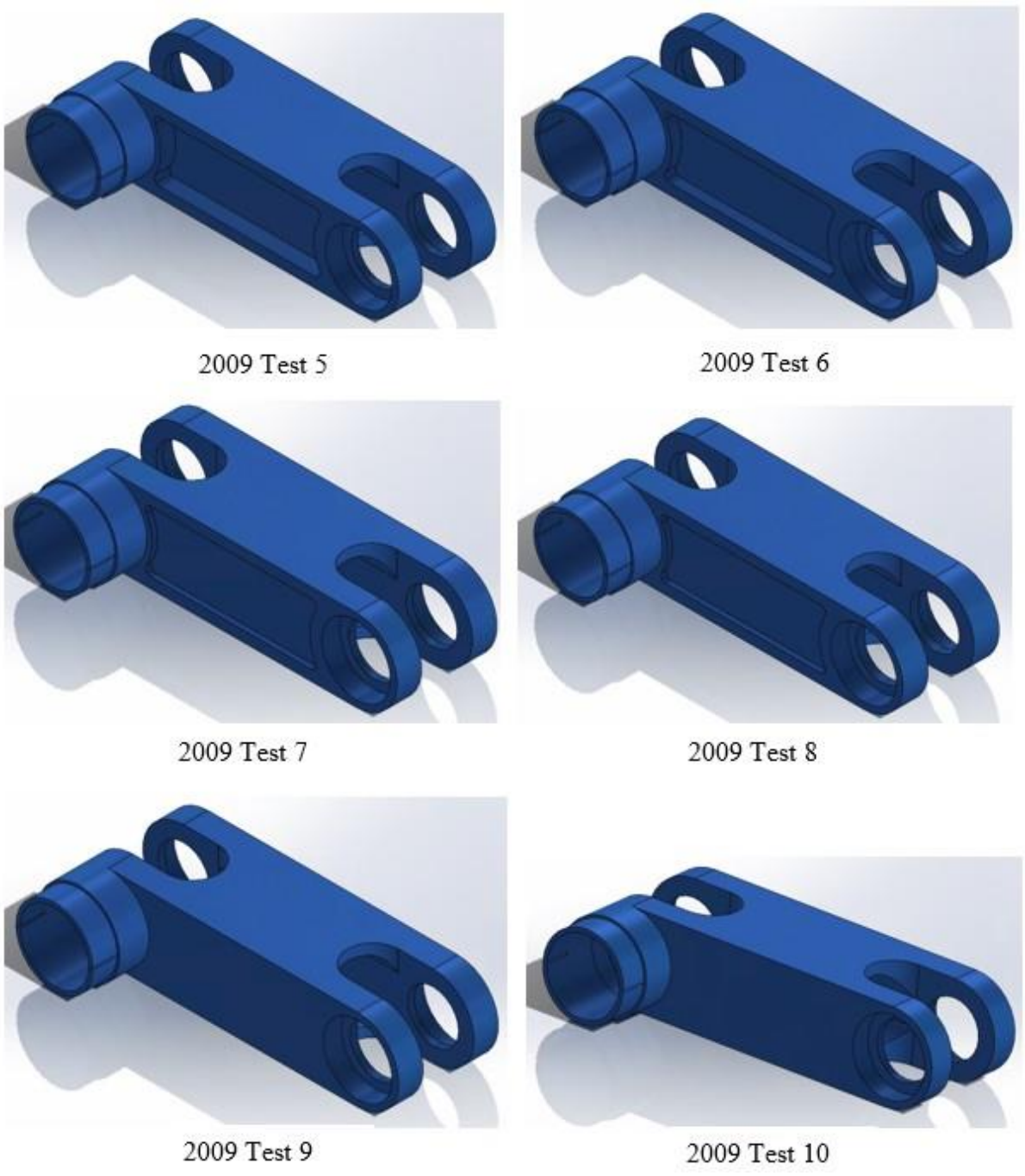

Figure B-8 Part 2009 images 2.

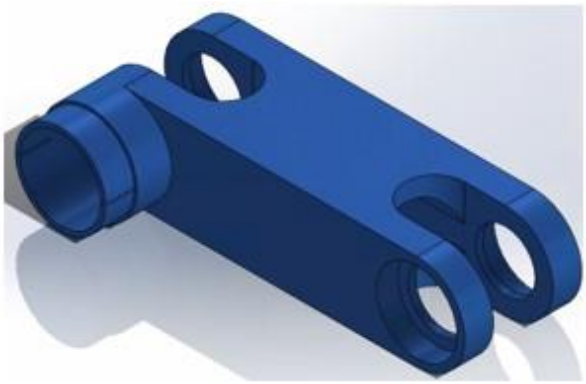

2009 Test 11

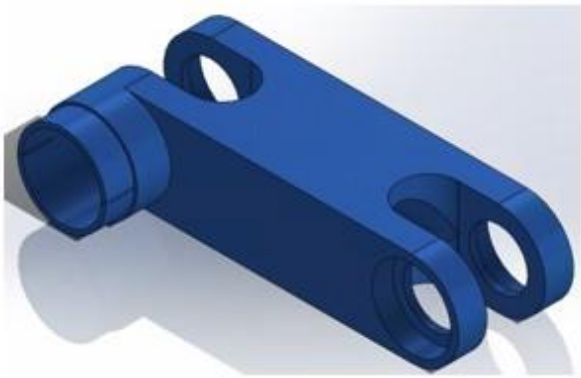

2009 Test 12

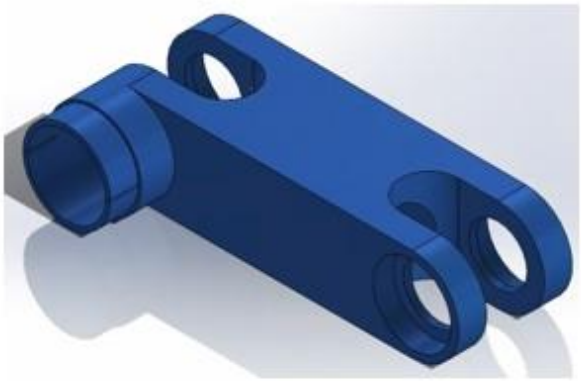

2009 Test 13

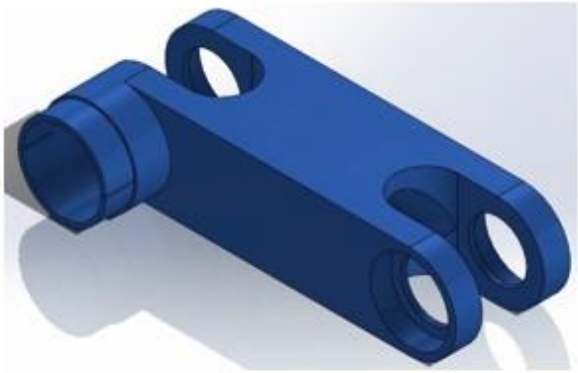

2009 Test 14

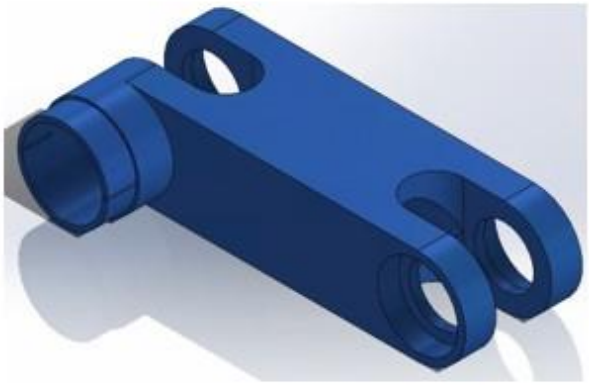

2009 Test 15

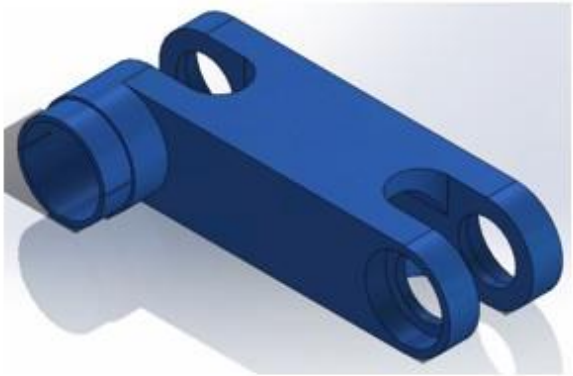

2009 Test 16

Figure B-9 Part 2009 images 3.

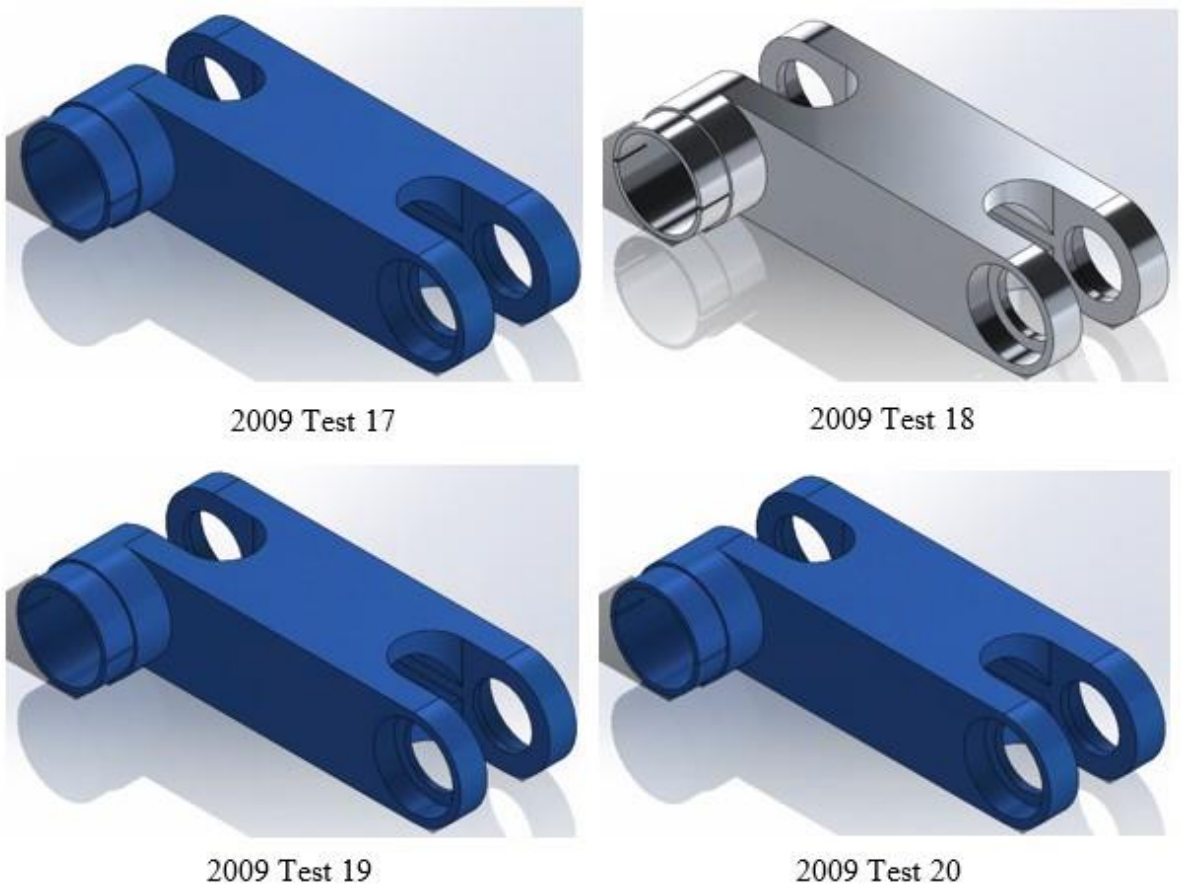

Figure B-10 Part 2009 images 4.

Table B-2 Summary of design alterations for part 2009.

Part 2009 Alterations						
Design #:	**Hole Shape:**	**Fillet (Rectangle):**	**Remaining Thickness (Rectangle):**	**Diameter (Circle):**	**Bearing Flange Thickness:**	**Side Profile Cutout Depth:**
1	Rectangle	3/8”	1/4”	N/A	4-mm	0”
2	Rectangle	3/8”	1/4”	N/A	5-mm	0”
3	Rectangle	3/8”	1/4”	N/A	5-mm	3/8”
4	Rectangle	3/8”	1/8”	N/A	5-mm	0”
5	Rectangle	3/8”	1/4”	N/A	4-mm	3/8”
6	Rectangle	3/8”	1/4”	N/A	4-mm	1/4”
7	Rectangle	3/8”	1/4”	N/A	4-mm	1/8”
8	Rectangle	3/8”	1/4”	N/A	5-mm	1/8”
9	Rectangle	1/4”	1/4”	N/A	4-mm	0”
10	Rectangle	1/2”	1/4”	N/A	4-mm	0”
11	Rectangle	3/8”	3/8”	N/A	4-mm	0”
12	Circle	N/A	N/A	1.22”	4-mm	0”
13	Circle	N/A	N/A	1”	4-mm	0”
14	Circle	N/A	N/A	1.22”	3-mm	0”
15	Circle	N/A	N/A	1.22”	5-mm	0”
16	Rectangle	3/8”	3/8”	N/A	5-mm	0”
17	Rectangle	1/2”	3/8”	N/A	5-mm	0”
18	Rectangle	1/2”	3/8”	N/A	4-mm	0”
19	Rectangle	1/2”	3/8”	N/A	3-mm	0”
20	Rectangle	7/16”	3/8”	N/A	4-mm	0”

Part 2010 Designs:

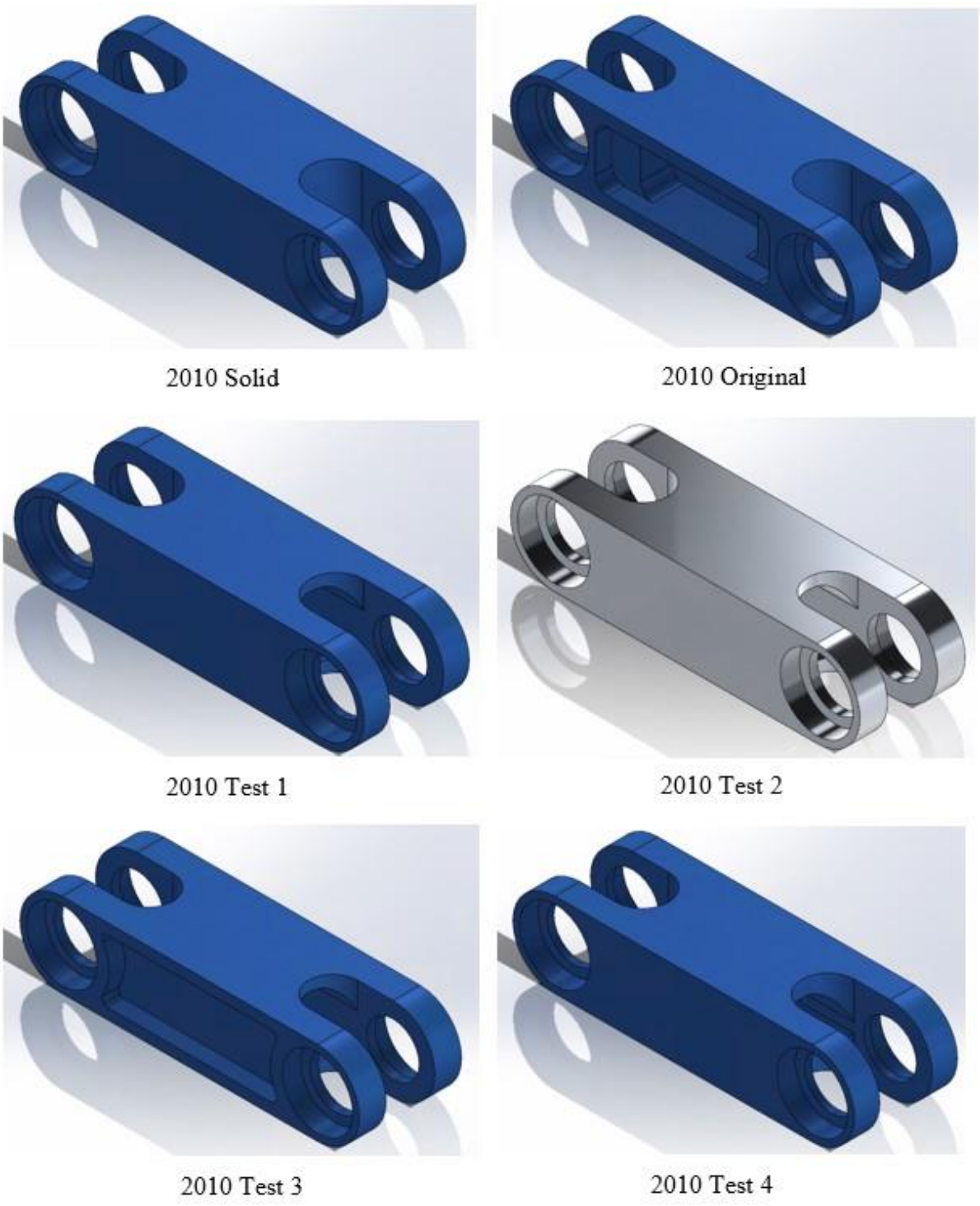

Figure B-11 Part 2010 images 1.

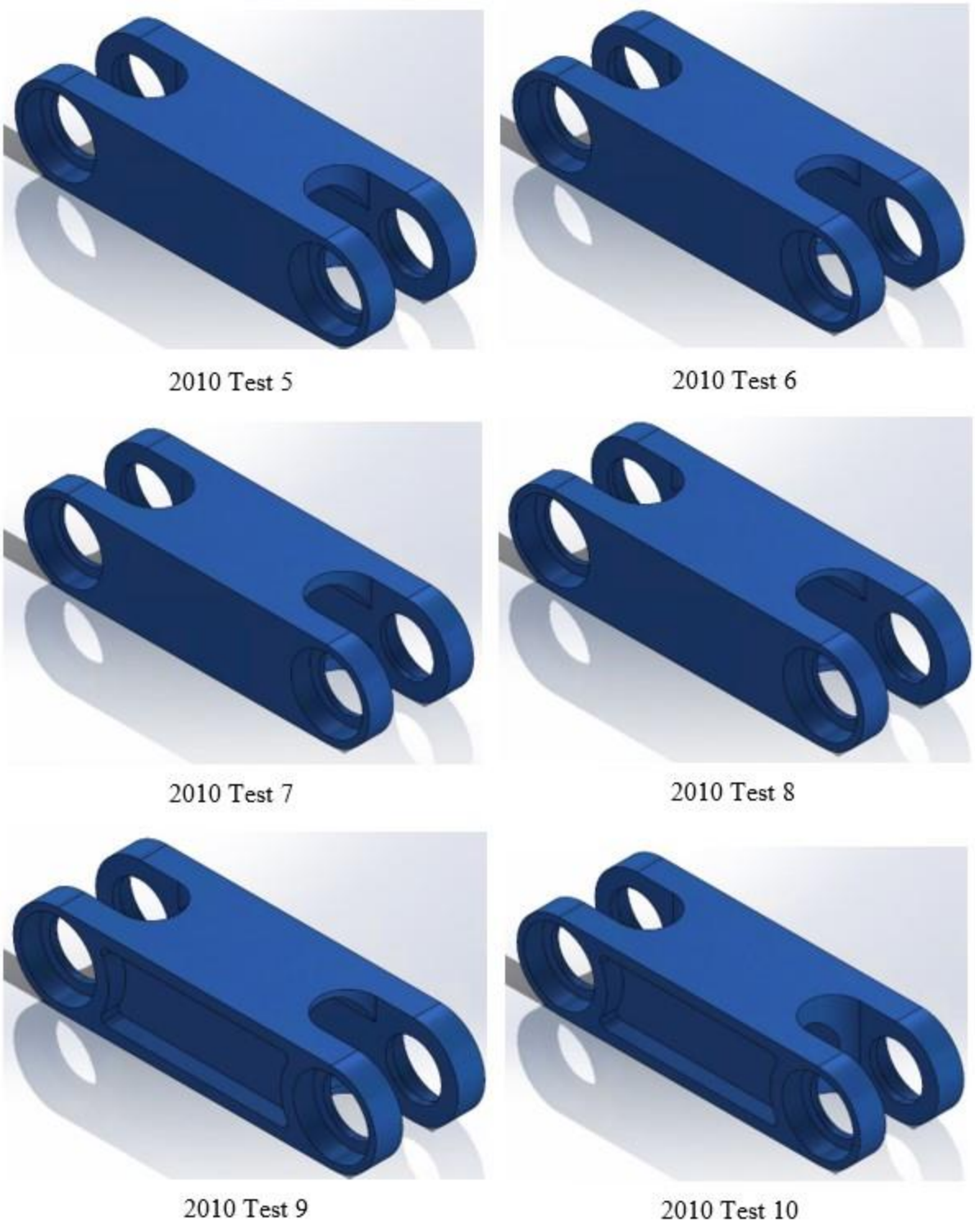

Figure B-12 Part 2010 images 2.

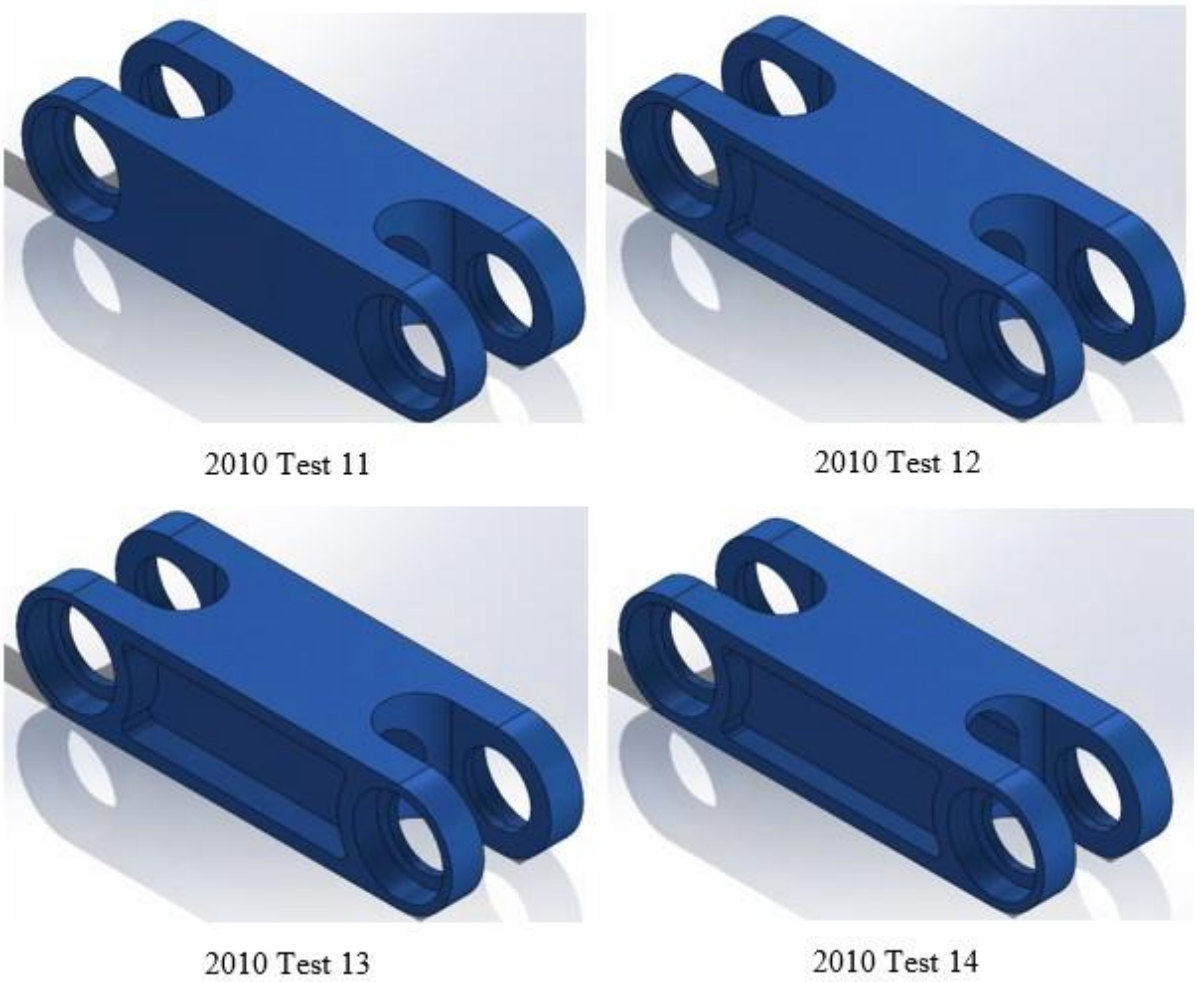

Figure B-13 Part 2010 images 3.

Table B-3 Summary of design alterations for part 2010. [1]This design is the only rectangle design in which the width does not align with the flanges.

Part 2010 Alterations						
Design #:	**Hole Shape:**	**Fillet (Rectangle):**	**Remaining Thickness (Rectangle):**	**Diameter (Circle):**	**Bearing Flange Thickness:**	**Side Profile Cutout Depth:**
1	Rectangle	3/8”	1/4”	N/A	4-mm	0”
2	Rectangle	3/8”	1/4”	N/A	5-mm	0”
3	Rectangle	3/8”	1/4”	N/A	5-mm	3/8”
4	Rectangle	1/2”	1/4”	N/A	4-mm	0”
5	Rectangle	3/8”	3/8”	N/A	4-mm	0”
6	Rectangle	1/4”	1/4”	N/A	4-mm	0”
7	Rectangle	3/8”	1/4”	N/A	3-mm	0”
8	Rectangle	3/8”	1/8”	N/A	3-mm	0”
9	Rectangle	3/8”	1/8”	N/A	4-mm	3/8”
10	Circle	N/A	N/A	1”	4-mm	3/8”
11	Circle	N/A	N/A	1”	4-mm	0”
12	Circle	N/A	N/A	1”	3-mm	3/8”
13	Circle	N/A	N/A	1”	4-mm	1/2”
14	Rectangle[1]	1/2”	3/16”	N/A	4-mm	3/8”